POLITECNICO DI MILANO
Energy Engineering Department

NUMERICAL ANALYSIS OF ENTROPY GENERATION IN A NON-UNIFORMLY HEATED TUBE

Supervisors: Prof. Luca Marocco
Prof. Luigi Colombo

Master Thesis of:
Pantilei Ianulov
Matr. **874870**

Academic year 2018/2019

Acknowledgments

In the first place I would like to thank my supervisors Prof. Luca Marocco and Prof. Luigi Colombo and express my gratitude to them for providing continuous support and guidance during my work.

Additionally, I am grateful to Politecnico di Milano University, particularly to Energy department, for providing very good level of education.

On the other hand, I would like to thank my colleagues and friends for their support throughout the entire of my studies. It wouldn't be possible without them.

Summary

In solar applications the tubes of the receiver are irradiated only from one side being the other one practically insulated. State of the art heat transfer fluids are thermal oils and molten salts, while recently also liquid metals have been also considered. One method of optimization of a solar tube heat exchanger is by using entropy minimization. A semi-empirical solution exists for the case of uniformly heated tube but not for more complex boundary conditions, as a strongly inhomogeneous wall heat flux. In this thesis OpenFOAM is used to perform Reynolds-Averaged-Navier-Stokes (RANS) simulations of forced convection to air and liquid metals flowing in a non-uniformly heated tube. The main objective is to numerically analyze entropy generation due to heat transfer and fluid flow for this geometry and boundary condition.

Contents

Index of Figures

Index of Tables

CHAPTER 1
INTRODUCTION

In engineering field there are a lot of technical applications where the heat transfer and the flow within the pipe is in high importance. Flow with low Prandtl number fluids are in particular interest since they represent the liquid metals. In Figure 1.1 you can observe the range of Prandtl numbers and corresponding fluids.

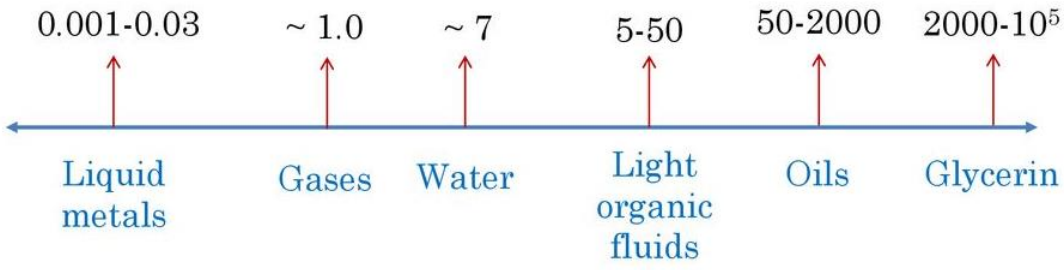

Figure 1.1. Prandtl Number of Fluids

For the gases the Prandtl number are about one, indicating that dissipation of momentum and heat are at the same level. However in liquid metals heat diffuses much quicker than in other fluids due to very low Pr number, which at the same time indicates that thermal boundary layer is much thicker in liquid metals relative to velocity boundary layer. This particular property can be benefited in solar applications. In this thesis particular attention will be fallen into Pr numbers 0.007, 0.025 and 0.046 corresponding to Sodium and Sodium-Potassium Alloys (Na, NaK), Lead Bismuth Eutectic (LBE) and Pure Lead (Pb), Mercury (Hg) consecutively.

In pipes most interesting region is near wall part, here viscous forces dominate thus the structure of the flow differs significantly from turbulent zone. In order to resolve this viscous layer strong refined computational grid is required which can lead to high computational costs. For this reason near wall models were developed in Computational

Fluid Dynamics. This models apply analytical wall functions near walls thus only core region of the flow is simulated which significantly reduces computational cost. Most of the analytical wall functions contain such parameter as turbulent Prandtl number that is considered as constant in most simulation codes although it increases towards the wall [1], Figure 1.2. In following simulations Kays mathematical model will be used to take the non-fixed value into account. As the Pr number increases the thermal boundary layer becomes thinner, which means essential transport mechanism for heat becomes closer and closer to the wall. Opposite happens for decreasing Pr number.

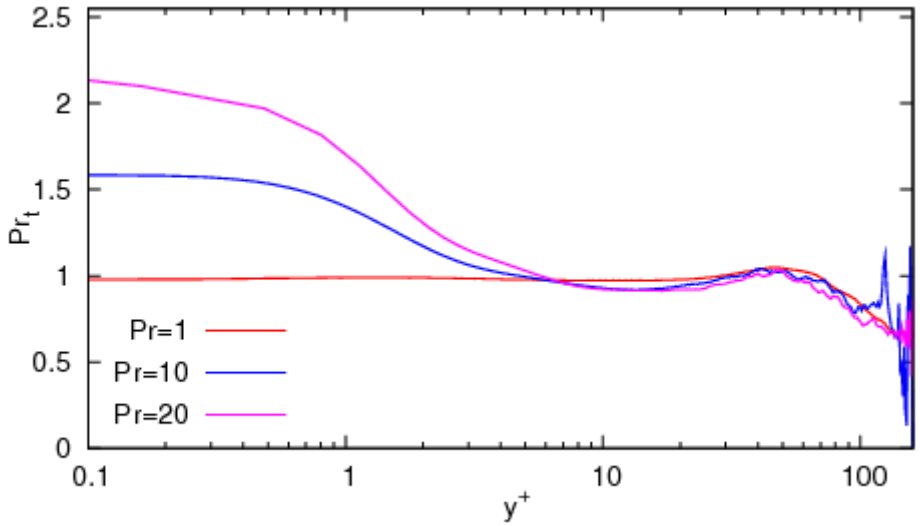

Figure 1.2. Turbulent Prandtl Number

Concentrated solar power systems are the energy systems where large area solar energy is concentrated in a small area with the help of mirrors or lenses. In CSP systems liquid metals are proposed to be used for being very efficient heat transfer media and resistant to high thermal loads. The tubes of a receiver of CSP are irradiated from one side while other side is practically insulated. One of the methods of optimization of solar tube heat exchangers is by using the minimization of entropy generation. Semi empirical solution exists for uniform heat flux on the wall of the tube, but for more complex boundary conditions such as inhomogeneous wall heat flux there are no any correlations. In current study OpenFoam open source CFD tool will be used to perform RANS simulations for non-uniform heated tube for different liquid metals. Objective of thesis is to numerically analyze entropy generation due to heat transfer and fluid flow with non-uniform heat flux.

CHAPTER 2
FUNDAMENTALS

2.1 Transport Equations

The investigation of heated and cooled fluid reduces to the fact that conservation of mass, momentum and energy have to be solved. The balance of mass and momentum, or in other words Navier-Stokes equations can be written in conservative form as [3]:

$$\frac{\partial \rho}{\partial t} + div(\rho \vec{u}) = 0$$

$$\frac{\partial (\rho \vec{u})}{\partial t} + div(\rho \vec{u}\vec{u}) = +\rho \vec{g} - grad(p) + div(f)$$

where f is viscous stress tensor;
The conservative equation of energy:

$$\frac{\partial (\rho e)}{\partial t} + div(\rho e \vec{u}) = -p\ div(\vec{u}) + div\big(k\ grad(T)\big) + \Phi + S_i$$

The computational analysis in this thesis acknowledges an incompressible, pressure driven, fully developed turbulent circular pipe flow.

2.2 Finite Volume Method

Equations defined above can't be solved analytically, they require numerical methods to be solved. Most widely used technique in commercial codes is finite volume method. The idea of this approach is to discretize the domain into finite set of control volumes, Figure 2.1, and for each volume cell general conservation for mass, momentum and energy equations are applied [3].

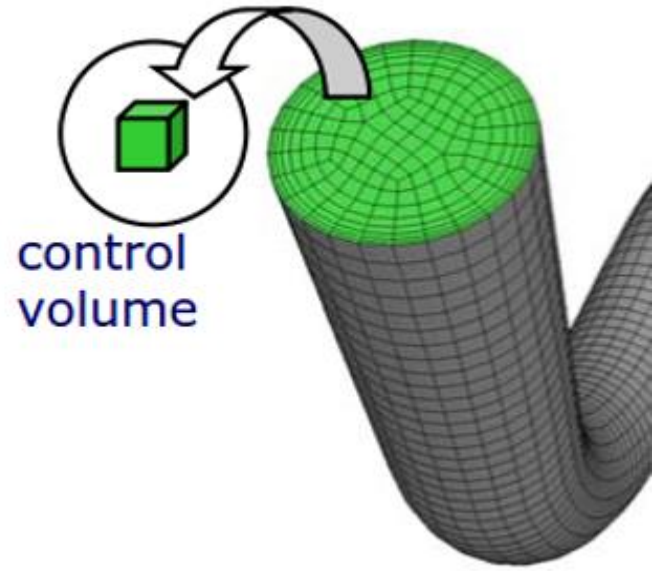

Figure 2.1 Control Volumes

General form of all equations can be written as:

$$\underbrace{\frac{\partial}{\partial t}\int_V \rho\phi dV}_{unsteady} + \underbrace{\oint_A \rho\phi V \cdot dA}_{convection} = \underbrace{\oint_A \Gamma\nabla\phi \cdot dA}_{diffusion} + \underbrace{\int_V S_\phi dV}_{generation}$$

where ϕ is

Equation	ϕ
continuity	1
x-mom.	u
y-mom.	v
z-mom.	w
energy	h

In differential form equations take general form shown below:

$$\frac{\partial(\rho\phi)}{\partial t} + div(\rho\phi\vec{u}) = div[\Gamma grad(\phi)] + S_\phi$$

The integral form of this differential equation can be demonstrated as follows:

$$\int_{CV}\frac{\partial(\rho\phi)}{\partial t}dV + \int_{CV} div(\rho\phi\vec{u})dV = \int_{CV} div[\Gamma grad(\phi)]dV + \int_{CV} S_\phi dV$$

Applying Gauss theorem:

$$\int_{CV}\frac{\partial(\rho\phi)}{\partial t}dV + \int_A \vec{n}\cdot(\rho\phi\vec{u})dA = \int_A \vec{n}\cdot\Gamma grad(\phi)dA + \int_{CV} S_\phi dV$$

Some of the problems in CFD can require just steady state solution, some of them can be time dependent. In first case our equations will have this form:

$$\int_A \vec{n} \cdot (\rho\phi\vec{u})dA = \int_A \vec{n} \cdot \Gamma grad(\phi)dA + \int_{CV} S_\phi dV$$

For time dependent problems:

$$\int_{\Delta T} \frac{\partial}{\partial t}\left(\int_{CV} \rho\phi dV\right)dt + \int_A \vec{n} \cdot (\rho\phi\vec{u})dA = \int_A \vec{n} \cdot \Gamma grad(\phi)dA + \int_{CV} S_\phi dV$$

Depending of the type of the problem the integral equations are discretized into a system of algebraic equations by using numerical methods and solved by iterative techniques. The solution of the flow field is defined at nodes inside each cell. The accuracy of solution is directly dependent on the density of the grid.

The conservation equations are more complex than they appear. They are nonlinear, coupled and difficult to solve. It is not easy to show with current mathematical tools that only one unique solution exists for particular boundary conditions. Navier-Stokes equations describe quite well the flow of Newtonian fluids but for only few very simple cases analytical solution is available.

2.3 Turbulence

2.3.1 General

Turbulence in fluid flow is defined as chaotic changes of pressure and velocity fields. It is characterized by three dimensionality, unsteadiness and seemingly random fluctuations. Although turbulent flow is considered chaotic it is well organized in coherent spatial structures, where large structures carry most energy, are highly influenced by the domain of the geometry and are responsible for mixing of mass, heat and momentum, while smaller structures are more universal and is not directly influenced by geometry of the domain.

Above mentioned structures are called eddy. Kolmogorov theory describes how the energy is transferred from big to smaller eddies. There are described three main turbulent length scales: Integral scale, Taylor scale, Kolmogorov scale, Figure 2.2.

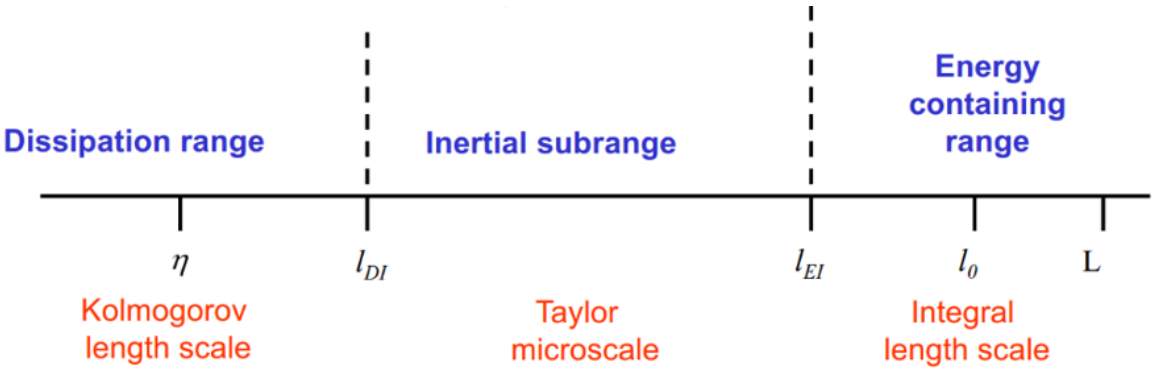

Figure 2.2. Turbulent Length Scales

Kolmogorov's theory is based on tree hypothesis [3]:

- Hypothesis of local isotropy, which says that at sufficiently high Re fluid flows the small scale turbulent motions ($l \ll l_0$) are statistically isotropic.
- First similarity hypothesis, which states that at sufficiently high Re fluid flows statistics of small scale motions ($l < l_{EI}$) have universal form and is defined by kinematic viscosity and turbulent dissipation rate.
- Second similarity hypothesis, which asserts that in every turbulent flow at sufficiently high Re, the statistics of the motion of scale in range $\eta \ll l \ll l_0$ have a universal form and is defined only by turbulent dissipation rate, independent of kinematic viscosity.

Energy transfer in fluid flow is described in Figure 2.3. Here we can see that most of the energy is contained in large eddies, subsequently large eddies transfer its energy into smaller one until Kolmogorov scale, where kinetic energy is dissipated into internal energy.

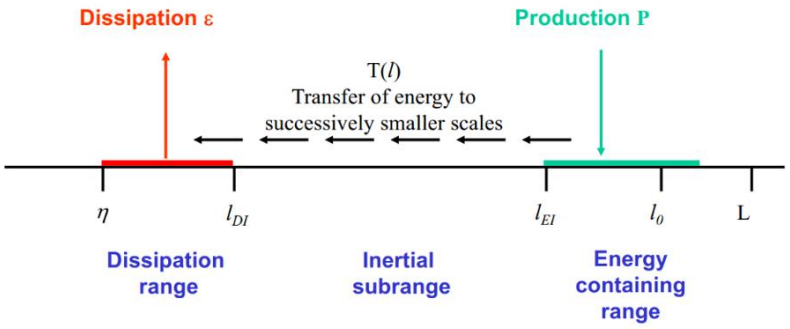

Figure 2.3. Energy Transfer in Fluid Flow

By knowing two parameters, kinematic viscosity and turbulent dissipation rate Kolmogorov length, time and velocity scales can be defined. Scales indicate smallest eddies where energy is dissipated.

$$Length\ scale\colon\ \eta = \left(\frac{\upsilon^3}{\epsilon}\right)^{\frac{1}{4}}$$

$$Velocity\ scale:\ u_\eta = (\epsilon\upsilon)^{\frac{1}{4}}$$

$$Time\ scale:\ \tau_\eta = \left(\frac{\upsilon}{\epsilon}\right)^{\frac{1}{2}}$$

$$Re_\eta = \frac{\eta u_\eta}{\upsilon} = 1$$

Kolmogorov Reynolds number Re_η of small eddies is equal to one, indicating that cascade proceeds to smaller and smaller scales until Re number is small enough for dissipation to take the place.

Dimension of large scale eddies is in direct proportion with turbulent kinetic energy and inversely proportional to turbulent dissipation rate:

$$l_0 \sim \frac{k^{\frac{3}{2}}}{\epsilon}$$

Hence, we can calculate the ratio of small and large scale eddies:

$$\frac{\eta}{l_0} \sim Re_L^{-\frac{3}{4}}$$

$$\frac{u_\eta}{u_0} \sim Re_L^{-1/4}$$

$$\frac{\tau_\eta}{\tau_0} \sim Re_L^{-1/2}$$

Hereof we can make one important conclusion, at high Re numbers the velocity and timescale of smallest eddies are much smaller compared with largest eddies. Moreover, at large Re numbers the range of intermediate scales will be wider.

The definition of turbulent kinetic energy is as follows:

$$k = \frac{1}{2} < u_i u_i > = \frac{1}{2}(\overline{u'^2} + \overline{v'^2} + \overline{w'^2})$$

In order to understand how energy is distributed among different scales we have to look at energy spectrum Figure 2.4, where $E(\kappa)$ is energy contained in eddies of size l and wave number κ [3].

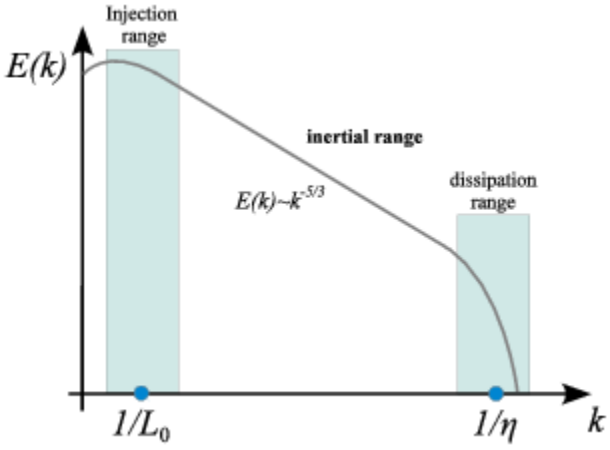

Figure 2.4. Energy Spectrum

Thus, another definition for turbulent kinetic energy can be demonstrated in this way:

$$k = \int_0^\infty E(\kappa) d\kappa$$

In 1941 Kolmogorov showed that:

$$\frac{\eta}{L_0} \approx Re_0^{-\frac{3}{4}} = \left(\frac{U_0 L_0}{\upsilon}\right)^{-\frac{3}{4}}$$

Hence, we can find the smallest eddy scale by knowing Reynolds number of the fluid flow.

Kolmogorov's theory is an asymptotic theory, the shape of the spectra can deviate from Kolmogorov's model for intermediate Re numbers. Kolmogorov's theory assumes that energy cascade is in one way, meaning that energy is transferred from large eddies to smaller one but in reality it is possible another way around, although, only small proportion of eddies are doing this way.

2.3.2Turbulence Models

For very few simple cases directly full unsteady Navier-Stockes equations can be solved which resolves all eddy scales, thus there is no need for any turbulence models. It is called DNS, direct numerical simulations. It is useful only as a research tool and feasible only for simple geometries. The model that solves large eddies and model small one is called LES, large eddy simulations. Eddies smaller than a mesh are modelled, it has a drawback, it is inherently unsteady. Most widely used turbulence model in industrial flows is RANS, Reynolds Averaged Navier-Stokes, which completely models the turbulence, Figure 2.5.a, thus drastically reduce amount of time and CPU required for simulations. Only this model is suitable for steady state solutions.

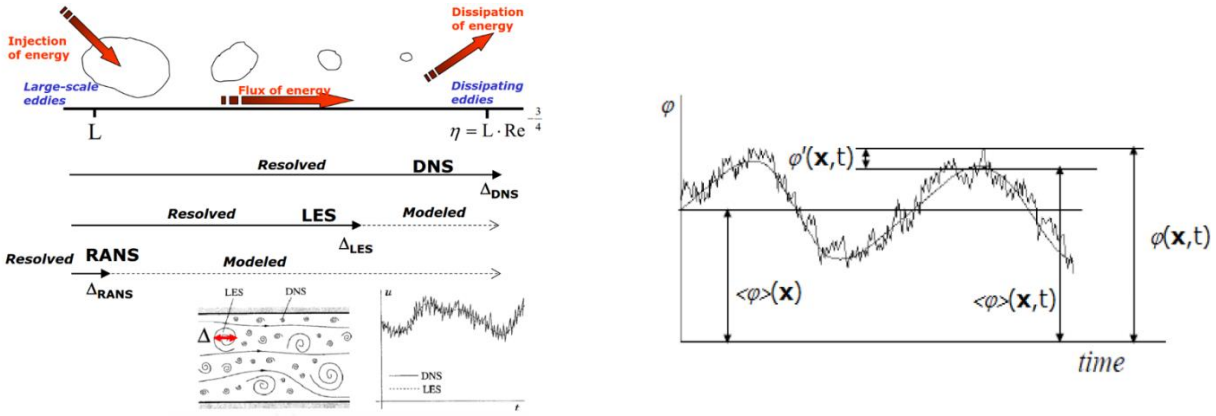

a) b)

Figure 2.5. Turbulence models

The idea behind RANS is that all components of the field are divided into fluctuating and mean components [9], Figure 2.5.b.

$$\varphi(\vec{x},t) = \Phi(\vec{x}) + \varphi'(\vec{x},t)$$

$$\Phi(\vec{x}) = \lim_{\Delta T \to \infty} \frac{1}{\Delta T} \int_{t}^{t+\Delta T} \varphi(\vec{x},t)dt$$

The root mean square (r.m.s.) values of velocity components are in particular importance because they are easily measured and they express the average magnitude of velocity fluctuation which is used in calculations of turbulent kinetic energy.

$$\varphi_{rms} = \left[\frac{1}{\Delta t}\int_{0}^{\Delta t}(\varphi')^2 dt\right]^{\frac{1}{2}} ; \quad \overline{(\varphi')^2} = \frac{1}{\Delta t}\int_{0}^{\Delta t}(\varphi')^2 dt \;\; ;$$

$$k = \frac{1}{2}\left(\overline{u'^2} + \overline{v'^2} + \overline{w'^2}\right) ;$$

Unsteady Reynolds-averaged Navier-Stokes equations for incompressible flow in scalar formulation have the following form:

$$\frac{\partial U}{\partial x} + \frac{\partial V}{\partial y} + \frac{\partial W}{\partial z} = 0$$

$$\frac{\partial U}{\partial t} + div\left(U\vec{U}\right) = -\frac{1}{\rho}\frac{\partial P}{\partial x} + \frac{\mu}{\rho} div[grad(U)] + \left[-\frac{\partial \overline{u'u'}}{\partial x} - \frac{\partial \overline{u'v'}}{\partial x} - \frac{\partial \overline{u'w'}}{\partial x}\right]$$

$$\frac{\partial V}{\partial t} + div\left(V\vec{U}\right) = -\frac{1}{\rho}\frac{\partial P}{\partial y} + \frac{\mu}{\rho} div[grad(V)] + \left[-\frac{\partial \overline{v'u'}}{\partial x} - \frac{\partial \overline{v'v'}}{\partial x} - \frac{\partial \overline{v'w'}}{\partial x}\right]$$

$$\frac{\partial W}{\partial t} + div\left(W\vec{U}\right) = -\frac{1}{\rho}\frac{\partial P}{\partial z} + \frac{\mu}{\rho} div[grad(W)] + \left[-\frac{\partial \overline{w'u'}}{\partial x} - \frac{\partial \overline{w'v'}}{\partial x} - \frac{\partial \overline{w'w'}}{\partial x}\right]$$

Fluctuating components in this set of equation are called Reynolds stresses, so in order to be able to compute turbulent flows with RANS equations it is necessary to predict this stresses.

$$Reynolds\ stresses: \boldsymbol{\tau_{ij}} = -\overline{\boldsymbol{\rho u_i' u_j'}}$$

Many turbulent models are developed to predict Reynolds stresses. Most common models are categorized based on number of additional transport equations to be solved together with RANS equations.

Classification of turbulent models:

- Based on Boussinesq hypothesis
  - Zero equation: Mixing length model
  - One equation: Spalart-Allmaras model
  - Two equations: k-ϵ model, k-ω
- Based on stress transport model
  - Zero equation: Algebraic RSM(Reynolds Stress Model)
  - Seven equations: RSM model

Boussinesq suggested that Reynolds stresses should be proportional to mean rates of deformation, meaning:

$$\boldsymbol{\tau_{ij}'} = -\overline{\boldsymbol{\rho u_i' u_j'}} = \boldsymbol{\mu_t}\left(\frac{\boldsymbol{\partial U_i}}{\boldsymbol{\partial x_j}} + \frac{\boldsymbol{\partial U_j}}{\boldsymbol{\partial x_i}}\right) - \frac{\mathbf{2}}{\mathbf{3}}\boldsymbol{\rho k \delta_{ij}}$$

where μ_t(turbulent viscosity) and k(turbulent kinetic energy per unit mass) are 2 unknowns.

In standard k-ϵ model Prandtl-Kolmogorov relation is used which describes the link between turbulent viscosity, turbulent kinetic energy and turbulent dissipation rate.

$$\mu_t = C_\mu \rho \frac{k^2}{\epsilon}$$

Extra two transport equations used in k-ϵ turbulence mode have the following general form:

$$\frac{\partial(\rho k)}{\partial t} + div\left(\rho k \vec{U}\right) = T_k + D_k + P_k$$

$$\frac{\partial(\rho \epsilon)}{\partial t} + div\left(\rho \epsilon \vec{U}\right) = T_\epsilon + D_\epsilon + P_\epsilon$$

Where T, D, P are transport, dissipation and production terms. The main difference between different turbulence models rise from the definition of generation and destruction terms, the method of calculation of turbulent viscosity, turbulent Pr number, which by the way is responsible for the diffusion of k and ϵ.

The idea behind turbulence stress transport model is that each Reynolds stress have its own transport equation, and that gives better prediction of Reynolds stresses but it requires more CPU resources and is less stable than k-ϵ model.

2.3.3Wall Functions

Near wall modelling plays significant role in CFD. Since the walls are the main sources for turbulence and vorticity the fluid have to be resolved properly in that zone, thus accurate representation of the flow near the wall region will determine how successful the turbulent flow will be predicted. Fluid flow region can be divided into four zones, viscous sublayer, buffer layer, fully turbulent or log-law region and outer layer, which completely depends on Reynolds number [3], Figure 2.6.

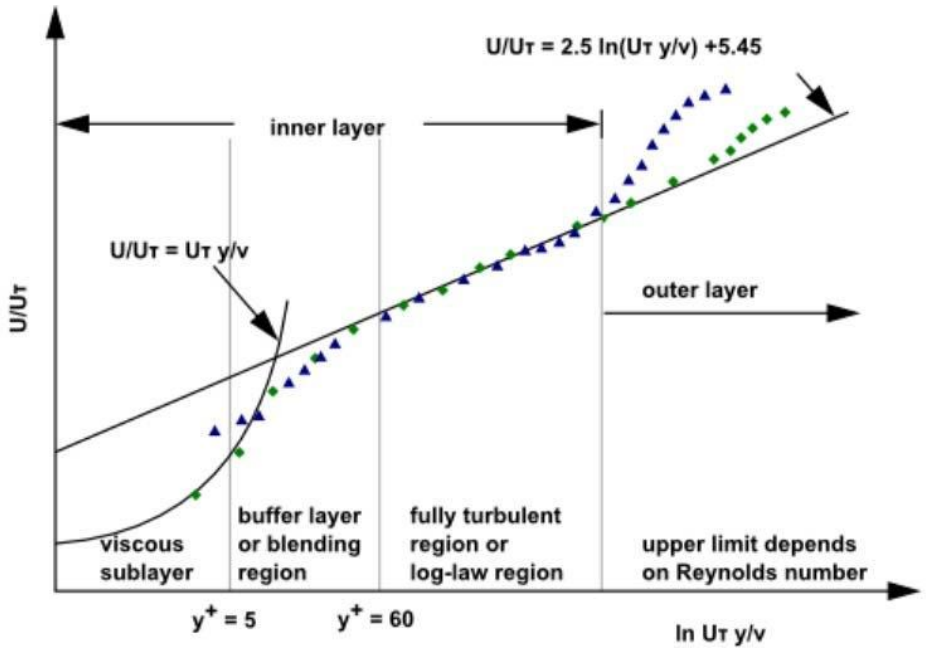

Figure 2.6. Wall functions

Wall functions are set of algebraic formulas that link solution variable at the near wall cells and corresponding quantities on the wall, they are required to model first tree layers thus significantly reducing the CPU time. They need to have first cell center of the grid point to lay in the logarithmic layer, meaning that at least $y^+ > 30$. Low Reynolds turbulence models resolve velocity profiles all the way to the wall, thus in this case it is required to have $y^+ \leq 1$.

2.4 Solution Schemes

Solution of transport equations for each velocity component contains few problems, the convection term in momentum equation contains non-linear quantity and there is no

separate equation for pressure. And the last one is the most complex issue. The linearized and discretized form of Navier-Stockes equation have the following form:

$$a_p u_p = \sum a_{nb} u_{nb} + b_p + (p_p + p_E) A_p$$

Where nonlinear quantities contribute to the a_p coefficient. P subscript represents main cell centre value and nb subscript symbolize neighbour cell values.

Here an iterative approach is required, meaning that if pressure field is correct the resulting field will satisfy continuity equation. Thus, it is required guess and correct technique to find the pressure field.

The pressure velocity coupling methods are based on guess of the right pressure, and the main ones are:

- SIMPLE (Semi Implicit Method for Pressure Linked Equations)
  - Very Robust
- SIMPLEC (SIMPLE Consistent)
  - Faster convergence for simple problems
- SIMPLER (SIMPLE Reduced)
- PISO (Pressure Implicit with Splitting of Operators)
  - Useful for unsteady flows and geometries having high skew mesh

2.5 Heat Transfer Phenomena

One of the most important non-dimensional number in heat transfer is the Prandtl number, which describes material property and is defined as ratio between momentum and thermal diffusivity.

$$Pr = \frac{c\mu}{\lambda} = \frac{\nu}{a} = \frac{momentum\ diffusivity}{thermal\ diffusivity}$$

Physical meaning of Prandtl number is that it relates thermal boundary layer and velocity boundary layer thickness, Figure 2.7 [2].

$$\frac{\delta_v}{\delta_T} \sim \sqrt{Pr}$$

From this mathematical definition we can make few conclusions, for fluids with Prandtl number close to unity thermal and momentum boundary layers have same thickness. If Prandtl number is much lesser than one, which describes properties of liquid metals, thermal boundary layer is much thicker that velocity boundary layer, in another words heat transfer occurs faster than momentum transfer in y direction.

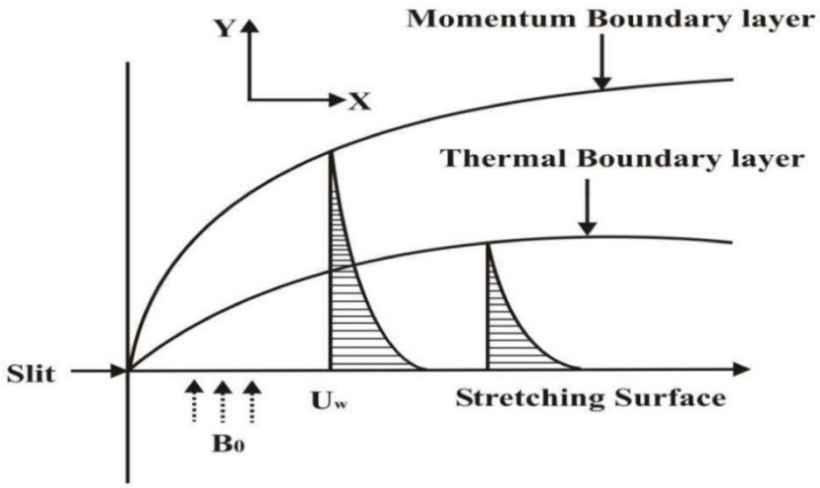

Figure 2.7. Boundary Layers

In Figure 2.8 we can observe which Prandtl number describes which type of fluid.

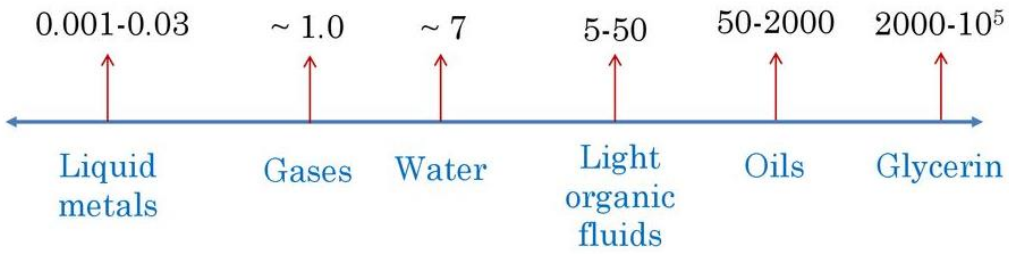

Figure 2.8. Fluids and corresponding Pr numbers

When it comes to turbulent flows turbulent Prandtl number appears as an analogy to molecular Prandtl number. It defines the ratio between eddy diffusivity of momentum and eddy conductivity shown as

$$Pr_t = \frac{\nu_t}{\alpha_t}$$

It correlates the turbulent transfer of momentum identified as turbulent stresses to turbulent transfer of heat identified as turbulent convective heat flux

$$\overline{u'v'} \leftrightarrow \overline{u'T'}$$

We should keep in mind that turbulent Pt_t number is not material property and based on experimental study it is in order of $Pt_t \sim 0.85$, but it can deviate a lot from this value close to the wall as previously mentioned.

Kays summarized experimental data of many authors and found that for Prandtl numbers between 0.7 and 64 the correlation

$$Pr_t = 0.85 + 0.7\left(\frac{\nu_t}{\nu}\right)Pr$$

operates quite well, but for lower Prandtl numbers subsequent correlation shows better results.

$$Pr_t = 0.85 + 2\left(\frac{\nu_t}{\nu}\right)Pr$$

Another important non-dimensional number in fluid dynamics is Nusselt number which can be defined locally or as a mean value. It represents the ratio of convective heat transfer to conductive heat transfer.

$$Nu_D = \frac{hD}{\lambda} = \frac{-\lambda \frac{\partial T}{\partial y}\,|_{y=0}}{\frac{\lambda}{D}(T_w - T_m)}$$

In many engineering applications analytical computation of Nusselt number is too complex therefore empirical correlations are frequently used.

2.6 Essentials of entropy and its generation

Efficient energy use in heat exchangers or whole power plants can be predicted if only together with first law of thermodynamics second one is also taken into account. By applying second law we can assess the amount of exergy present in the system which depends on the amount of entropy generated. Hence, heat exchanger producing lesser entropy due to irreversibilities will destruct lesser available work leading to higher efficiency of the system. Thus entropy generated can be considered as efficiency parameter. For instance, pipe with small cross section will encounter small temperature gradients leading to smaller entropy generation due to heat transfer but from another hand due to high pressure drops the entropy generation due to friction will be high. So overall performance can be evaluated only by linking this two terms and estimating total entropy production rate which should be as small as possible.

Entropy is a state variable and in specific form has following unit J/kgK. For single phase has form demonstrated below [5]:

$$\rho\left(\frac{\partial s}{\partial t} + u\frac{\partial s}{\partial x} + v\frac{\partial s}{\partial y} + w\frac{\partial s}{\partial z}\right) = div\left(\frac{\vec{q}}{T}\right) + \frac{\Phi}{T} + \frac{\Phi_\theta}{T^2}$$

Here two production terms are included Φ and Φ_θ. There is no need to solve this equation in order to determine entropy field, since s is a function of pressure and temperature $s = s(p, T)$. Thus, once temperature and pressure fields are known entropy can be determined as a post processing quantity.

Time averaged equation have to be considered in order to determine mean entropy field, thus Reynolds Averaged Navier Stokes approach have to be considered by splitting the equation quantities into mean and fluctuating parts [5]:

$$s = \bar{s} + s' \qquad\qquad u = \bar{u} + u'$$

Hence, time averaged equation takes following form:

$$\rho\left(\frac{\partial \bar{s}}{\partial t}+\bar{u}\frac{\partial \bar{s}}{\partial x}+\bar{v}\frac{\partial \bar{s}}{\partial y}+\bar{w}\frac{\partial \bar{s}}{\partial z}\right)=\overline{div\left(\frac{\vec{q}}{T}\right)}-\rho\left(\frac{\partial \overline{u's'}}{\partial x}+\frac{\partial \overline{v's'}}{\partial y}+\frac{\partial \overline{w's'}}{\partial z}\right)+\overline{\left(\frac{\Phi}{T}\right)}+\overline{\left(\frac{\Phi_\theta}{T^2}\right)}$$

Entropy production terms can be determined in two ways. If we consider equation for laminar flow the first method will be determination in detail the entropy generation terms and calculating them directly, which will be called direct method. The second method consists on the idea of equating of all entropy generation to the rest part of the equation, which can be calculated from known velocity, pressure and temperature fields, and current method is called indirect one [5].

In case of turbulent flow equation has two additional turbulent terms, thus, overall we can divide entropy production by dissipation into two terms: viscous dissipation ($S_{gen,fric,mean}$) and turbulent dissipation ($S_{gen,fric,fluc}$).

$$\overline{\left(\frac{\Phi}{T}\right)}=S_{gen,fric,mean}+S_{gen,fric,fluc}$$

The first term represents dissipation in mean flow field, second describes dissipation by turbulence.

Where they can be defined as:

$$S_{gen,fric,mean}=\frac{\mu}{\bar{T}}\left[2\left\{\left(\frac{\partial \bar{u}}{\partial x}\right)^2+\left(\frac{\partial \bar{v}}{\partial y}\right)^2+\left(\frac{\partial \bar{w}}{\partial z}\right)^2\right\}+\left(\frac{\partial \bar{u}}{\partial y}+\frac{\partial \bar{v}}{\partial x}\right)^2+\left(\frac{\partial \bar{u}}{\partial z}+\frac{\partial \bar{w}}{\partial x}\right)^2+\left(\frac{\partial \bar{v}}{\partial z}+\frac{\partial \bar{w}}{\partial y}\right)^2\right]$$

$$S_{gen,fric,fluc}=\frac{\mu}{\bar{T}}\left[2\left\{\overline{\left(\frac{\partial \bar{u}}{\partial x}\right)^2}+\overline{\left(\frac{\partial \bar{v}}{\partial y}\right)^2}+\overline{\left(\frac{\partial \bar{w}}{\partial z}\right)^2}\right\}+\overline{\left(\frac{\partial \bar{u}}{\partial y}+\frac{\partial \bar{v}}{\partial x}\right)^2}+\overline{\left(\frac{\partial \bar{u}}{\partial z}+\frac{\partial \bar{w}}{\partial x}\right)^2}+\overline{\left(\frac{\partial \bar{v}}{\partial z}+\frac{\partial \bar{w}}{\partial y}\right)^2}\right]$$

Analogously we can divide entropy production due to heat transfer into mean component ($S_{gen,heat,mean}$) due to time mean temperature gradients and fluctuating component ($S_{gen,heat,fluc}$) due to gradients of temperature fluctuations.

$$\overline{\left(\frac{\Phi_\theta}{T^2}\right)}=S_{gen,heat,mean}+S_{gen,heat,fluc}$$

where they can be defined as:

$$S_{gen,heat,mean}=\frac{\lambda}{\bar{T}^2}\left[\left(\frac{\partial \bar{T}}{\partial x}\right)^2+\left(\frac{\partial \bar{T}}{\partial x}\right)^2+\left(\frac{\partial \bar{T}}{\partial x}\right)^2\right]$$

$$S_{gen,heat,fluc}=\frac{\lambda}{\bar{T}^2}\left[\overline{\left(\frac{\partial \bar{T}}{\partial x}\right)^2}+\overline{\left(\frac{\partial \bar{T}}{\partial x}\right)^2}+\overline{\left(\frac{\partial \bar{T}}{\partial x}\right)^2}\right]$$

Overall in time averaged entropy equation appears four groups of entropy production terms:

- $S_{gen,fric,mean}$→ entropy generation by direct dissipation
- $S_{gen,fric,fluc}$→entropy generation by indirect dissipation
- $S_{gen,heat,mean}$→entropy generation due to mean temperature gradients
- $S_{gen,heat,fluc}$→entropy generation due to fluctuating temperature gradients

The mean terms of entropy generation can be calculated from known mean temperature and velocity fields. Fluctuating terms cannot be neglected and should be exposed to turbulence modelling. Since almost all turbulence models include turbulent dissipation rate ϵ the modelling proposed by Kock and Herwig [14] can be applicable:

$$S_{gen,fric,fluc} = \frac{\rho\epsilon}{\bar{T}}$$

$$S_{gen,heat,fluc} = \frac{\alpha_t}{\alpha} S_{gen,heat,mean}$$

Knowing the field values of each terms and integrating it overall of the control volume the total entropy produced can be calculated, which can be our target.

Due to steep gradients of T near to wall the entropy generation will accumulate at that regions, so in order to resolve that part of field or dense numerical grid have to be produced, or wall functions for entropy field should be used, which are defined as analytical expressions and are described in Kock [5]. In case if we use Low Reynolds Number turbulence models numerical grid will be fine near the wall so there will be no need for wall functions.

All of the information provided above are related with direct method of entropy calculation but few words have to be told about indirect method, which in some cases can be useful. So the entropy production in turbulent flow will be the sum of $\overline{\left(\frac{\Phi}{T}\right)}$ and $\overline{\left(\frac{\Phi}{T^2}\right)}$ terms. Mathematically indirect method can be defined in the following way:

$$S_{gen} = \overbrace{\overline{\left(\frac{\Phi}{T}\right)} + \overline{\left(\frac{\Phi}{T^2}\right)}}^{Generation} = \overbrace{\rho\left(\frac{\partial\bar{s}}{\partial t} + \bar{u}\frac{\partial\bar{s}}{\partial x} + \bar{v}\frac{\partial\bar{s}}{\partial y} + \bar{w}\frac{\partial\bar{s}}{\partial z}\right)}^{\text{Convection}} - \overbrace{div\left(\frac{\vec{q}}{T}\right)}^{\text{Molecular Flux}} +$$

$$\overbrace{\rho\left(\frac{\partial\overline{u's'}}{\partial x} + \frac{\partial\overline{v's'}}{\partial y} + \frac{\partial\overline{w's'}}{\partial z}\right)}^{\text{Turbulent Flux}}$$

Turbulent flux term can be modelled analogous to turbulent heat flux in energy equation, thus the local rate of entropy production can be determined by computing the right hand side of equation once the turbulence model of turbulent flux is known or neglected, which can be justified only in some particular cases at very high Re number flows. As it was mentioned before the indirect method can provide only total entropy generation rate but not separate term ones.

Bejan [6] showed that for uniform heat flux with neglecting the turbulent heat flux and with Prandtl number equal to one the entropy generation in control volume will have following form:

$$\iiint S_{gen} dV = -\frac{8m^4 c_p \ln\left(\frac{T_2}{T_1}\right)}{\pi^3\rho^2 D^6 q_w^2} c_f + \frac{q_w^2 D^2 \pi L}{\lambda T_1 T_2} Nu^{-1}$$

Which with Blasius and Dittus-Boelter correlations:

$$\text{Blasius} \rightarrow c_f = 0.316\text{Re}^{\frac{1}{5}}$$

$$Dittus - Boelter \rightarrow \text{Nu} = 0.023\text{Re}^{0.8}\text{Pr}^{0.4}$$

will have the form:

$$\iiint S_{gen} dV = C_1 Re^{5.75} + C_2 Re^{-1.8}$$

where C_1 and C_2 are constants.

Following indirect method can be used to understand the physics of complex processes and the ways to reduce overall entropy generation in technical devices but if more superior analysis will be required then direct method should be applied. One important thing should be kept into the mind, entropy generated multiplied with ambient temperature gives us the useful energy that is forever lost.

CHAPTER 3
APPROPRIATE TURBULENT MODEL

In current part of the project individual turbulent models will be evaluated by application to the pipe flow over a range of Reynolds numbers. The objective is to determine best suited turbulence model for particular our case. Fife different turbulence models were taken into account. Two high Reynolds number (HRN) and tree low Re number (LRN) models: Launder-Shaurma k-epsilon, v2f, k-omega SST, Realizable k-epsilon and k-epsilon RNG consecutively.

Geometry of pipe is very simple, so structured mesh were generated for our case, Figure 3.1. This type of the mesh is aligned with the flow which typically leads to better results and faster convergence. Moreover, lesser number of cells are used in computation. More detailed mesh information can be seen in Table 3.1. As we can observe LRN models' mesh requires higher number of cells due to denser mesh near the wall, moreover higher the Reynolds number of the flow greater the number of cells. Particular attention have to be paid to y+ when we use different models, LRN has need to $y^+ \sim 1$, meanwhile, HRN models require $y^+ \geq 30$

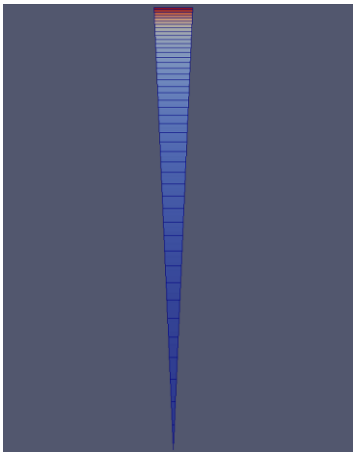

Figure 3.1. 2D Mesh

Table 3.1. Mesh Information

	Number of Cells				
	Turbulence models				
Re	LaunderShaurmaKe	kOmegaSST	v2f	realisableKE	RNGkEpsilon
10000	606	606	606	66	66
40000	1806	1806	1806	186	186
80000	3006	3006	3006	366	366
120000	3966	3966	3966	486	486
200000	9006	9006	9006	846	846
500000	13206	13206	13206	1806	1806
Re	***Max y+***				
10000	0.78	0.79	0.8	32	32
40000	0.89	0.95	0.92	33	33
80000	1.01	0.99	1.02	31	31
120000	1.11	1.01	1.11	33	33
200000	0.75	0.9	0.77	30	30
500000	1.2	1.28	1.2	33	33

Substantial influence on the solution renders the discretization schemes and the solution algorithms. For the incompressible fluids there are two important algorithms PISO and SIMPLE. PISO performs well for unsteady cases, SIMPLE operate better with steady cases as previously mentioned. In our situation there is a steady case, so SIMPLE algorithm will be selected. Considering the discretization schemes bounded Gauss linear method has been chosen. Gauss linear is preferred against UPWIND scheme because it reduces numerical diffusion, although completely it cannot be avoided due to discretization. Boundedness is preserved with this scheme, thus over and undershooting are avoided leading to more physical results.

Although HRN models can give good description of the flow in fully turbulent region they apply wall functions in a viscous, buffer and log-law regions which can perform well for Pr numbers close to the unity and rather simple geometries. Moreover, to obtain values of temperature and velocity fields near wall requires interpolation of the points according to the wall functions.

We are interested in modeling the flow of liquid metals (very low Pr number) where wall functions were found to not give right profile. It is required to resolve in detail whole fluid domain, thus LRN models seem to be more utile due to the fact that they are applied to the whole fluid region, including near wall region. Wall functions for both types of turbulence models are shown in Table 3.2.

Table 3.2. Wall Functions

Low Re number turbulence models' wall BC							
	alphat	epsilon	k	nut	p	T	U
type	fixedValue	fixedValue	kLowReWallFunction	nutLowReWallFunction	zeroGradient	fixedGradient	noSlip
value	uniform 1e-10	uniform 1e-9	Uniform 1e-10	Uniform 0		depends on Re number	
High Re number turbulence models' wall BC							
	alphat	epsilon	k	nut	p	T	U
type	fixedValue	epsilonWallFunction	kqRWallFunction	nutkWallFunction	zeroGradient	fixedGradient	noSlip
value	uniform 1e-10	uniform 5.3905e-4	Uniform 0.00375	Uniform 0		depends on Re number	

Understanding which turbulent model is more suitable for our case requires the data or correlations already available so that our models can be compared. Nusselt numbers were computed using each fife models for Pr=1 and the results were compared with experimental correlation of Gnielinski, Figure 3.2, which shows best performance for Prandtl numbers close to unity. As it can be observed some models overpredict Nusselt values, some of them underpredict.

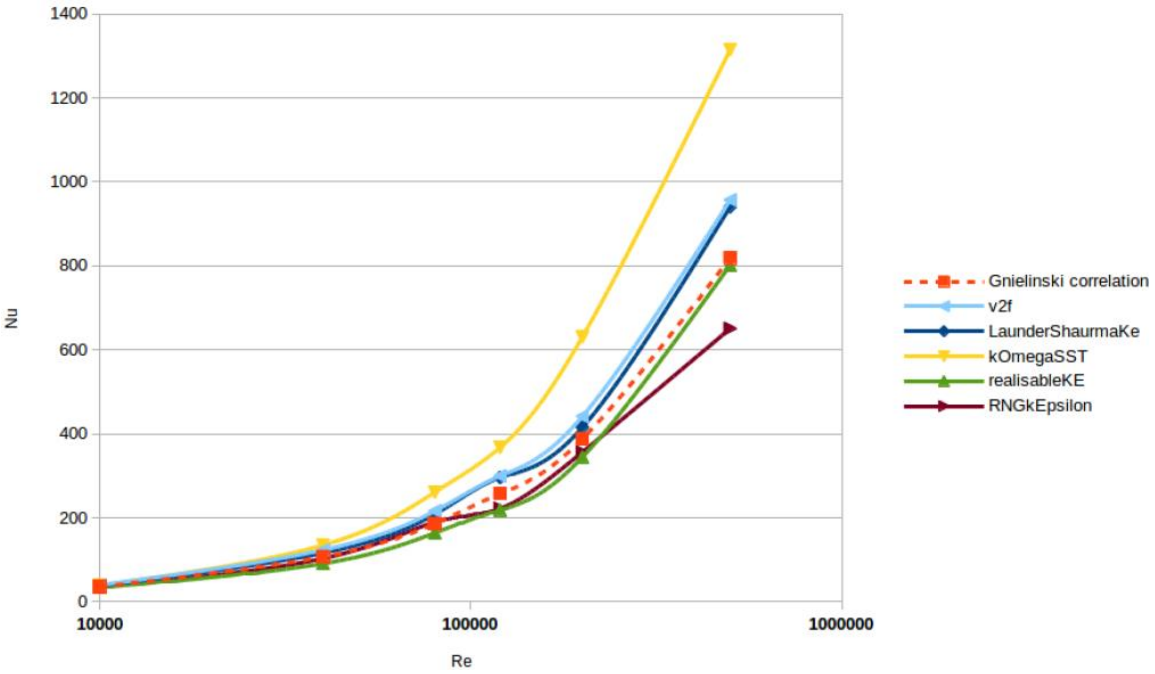

Figure 3.2. Correlations and Simulations results

Before jumping into conclusion of which model performs better and to judge about the correctness of the solution convergence have to be checked. Residuals of the case with $Re = 200000$ and LS turbulence model can be seen in Figure 3.3. In our case we are interested only in U_z velocity component and temperature residuals, they seem to be low but not low enough, so it has been monitored the value of the temperature at random cell center and Nu number, this results can be observed in Figure 3.4, 3.5, thus we can speak about converged solution. Other mean velocity components have very small values since main flow direction is in z direction.

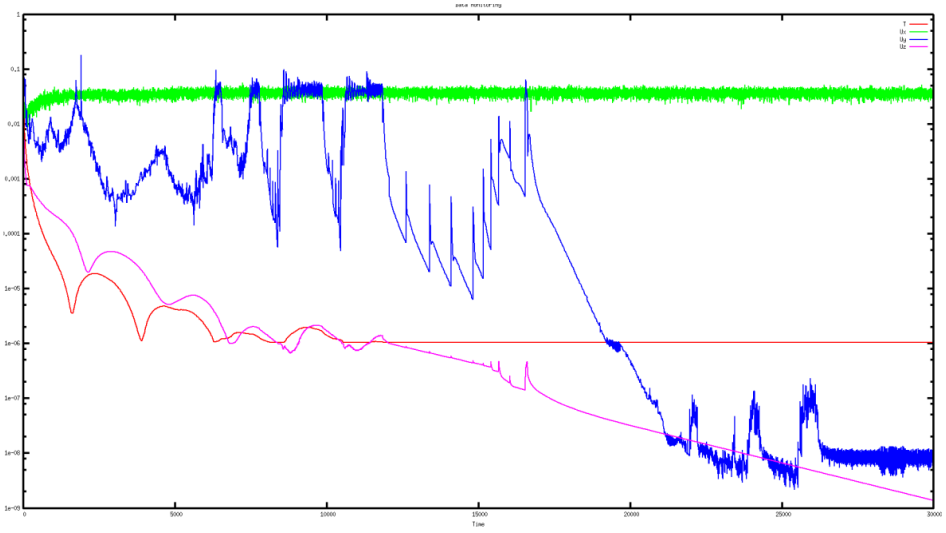

Figure 3.3. Residuals

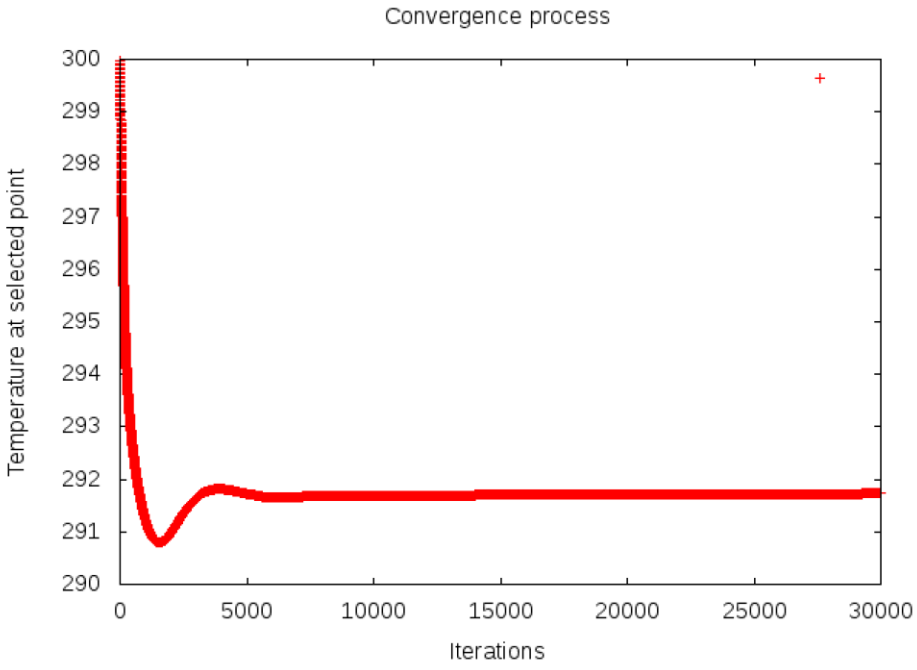

Figure 3.4. Convergence of Temperature

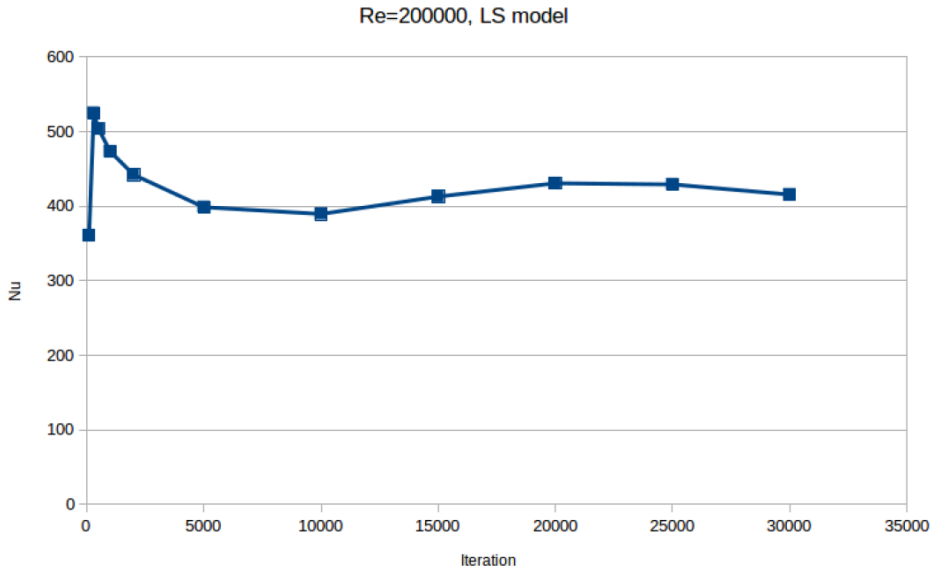

Figure 3.5. Convergence Nusselt number

As a result of simulations two turbulence models provide results with the smallest error. First is Realisable k-epsilon, which is HRN model, with a maximum error 15.33%, but as previously said HRN models cannot correctly evaluate wall region especially for low Prandtl number fluids. Second one is Launder-Shaurma k-epsilon, which is LRN model, with a maximum error of 15%. Furthermore, from Figure 3.2 we can observe that $v2f$ model results are very close to Launder-Shaurma model. Bar chart, Figure 3.6, demonstrates us the relative errors of different turbulence models, hence, we can judge the performance of each model related with our case.

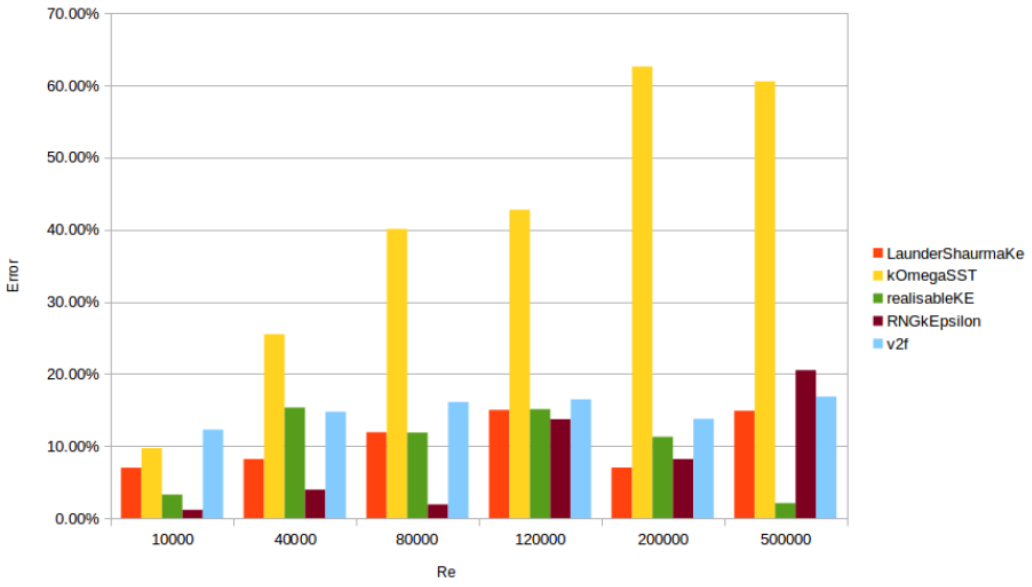

Figure 3.6. Relative Errors of Models

In our application case we are interested in heat transfer, it is clear that in case of laminar flow there is a linear relationship between flow temperature and wall distance:

$$T^+ = Pr\, y^+$$

Nevertheless, when flow becomes turbulent and Pr number deviates a lot from unity this mathematical relationship becomes nonlinear. To be able to make numerical simulations of heat transfer between fluid and solid this relationship have to be mathematically modeled, otherwise, numerical grid have to be sufficiently refined so that first grid cell lies in linear region. Thus, before concluding which model will be used in simulation of liquid metals temperature and velocity profiles will be examined in contrast with Reichardt and Kader correlations. Reichardt correlation were developed for velocity profile of the turbulent flow [7] and has the following form:

$$u^+ = \frac{1}{\kappa}\ln(1+\kappa y^+) + 7.8\left[1 - e^{-\frac{y^+}{11}} - \frac{y^+}{11}e^{-\frac{y^+}{3}}\right]$$

where κ is the Von Karman constant and here is equal to 0.42.

Similarly Kader correlation were developed for temperature profile of the turbulent flows [7]:

$$T^+ = Pr\, y^+ e^{-L} + (2.12\ln(1+y^+) + \beta)e^{-\frac{1}{L}}$$

where

$$L = \frac{[0.01(Pr\, y^+)^4]}{[1 + 5\mathrm{Pr}^3\mathrm{y}^+]}$$

$$\beta = \left(3.85 Pr^{\frac{1}{3}} - 1.3\right)^2 + 2.12\ln(Pr)$$

You can notice in Figure 3.7 that Launder-Shaurma k-epsilon describes quite well both velocity and temperature fields in whole domain. Whereas in realizable k-epsilon model in order to obtain values of velocity and temperature field near wall, more precisely for $y^+ < 30$, requires wall function employment and interpolation of values according to wall function laws, which is done in Figure 3.7 d). Mesh does not contain field values for $y^+ < 30$ in comparison with Launder Shaurma k-epsilon model. Although there are advantages of Launder Shaurma model it has one drawback, it requires very fine mesh near wall, so that $y^+ \leq 1$, especially for high Re number flows, hence a lot of iterations are needed for the convergent solutions.

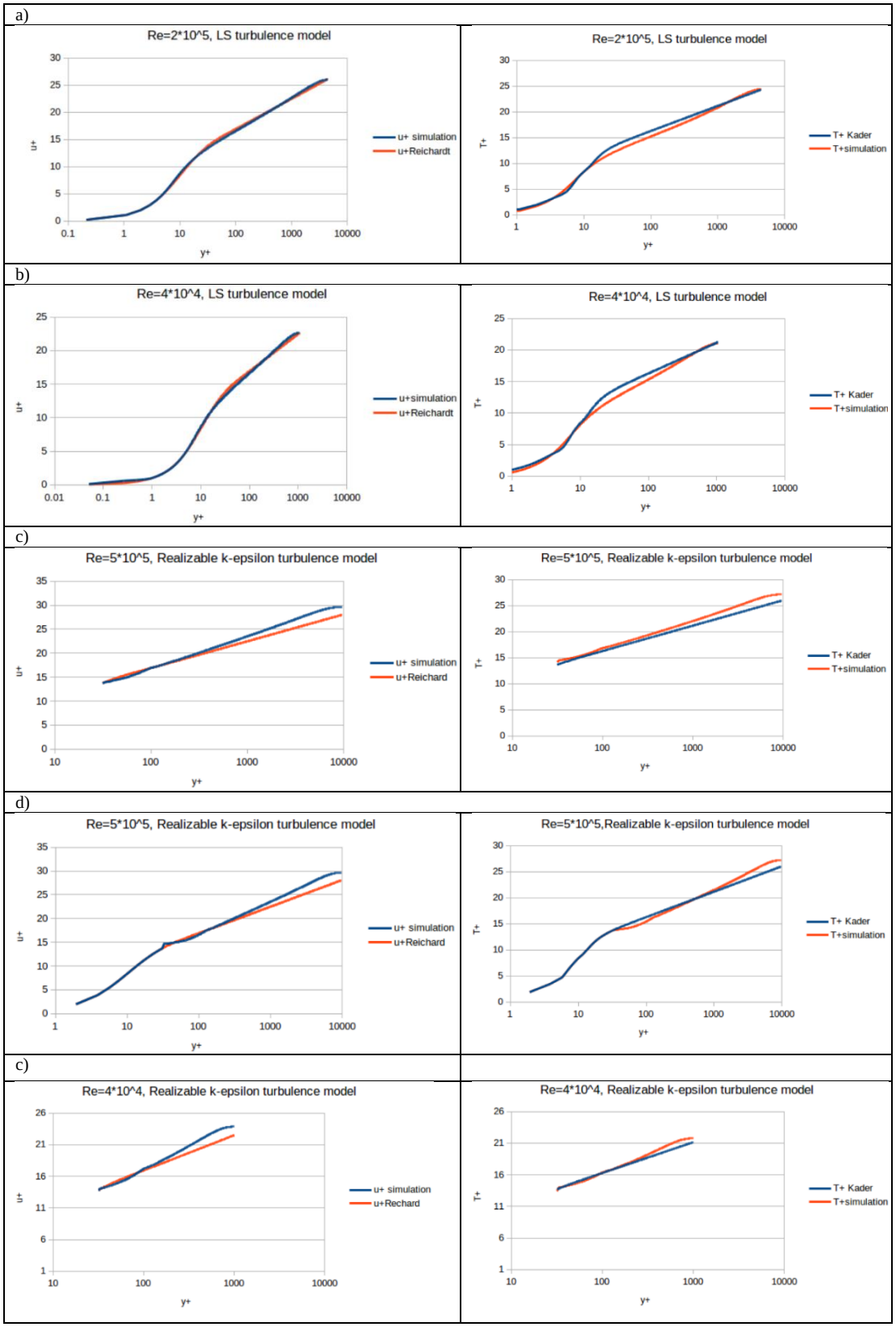

Figure 3.7. Simulation and Mathematical Models' Boundary Layers

Hereafter we will be using Launder-Shaurma turbulence model since it showed its advantages over other considered turbulence models and it is best suited for our further simulations.

Before proceeding with Launder-Shaurma model few more things will be discussed. In Low Reynolds Number turbulence models in the direction normal to the wall it is mandatory to have first cell center with $y^+ \leq 1$ and at least 5 to 10 cells within $y^+ = 20$ in order to correctly describe viscous sublayer. From the Figure 3.8 we can observe that this condition is satisfied. Within $y^+ = 20$ lay 10 and 14 cells corresponding to $Re = 10000$ and $Re = 200000$ respectively.

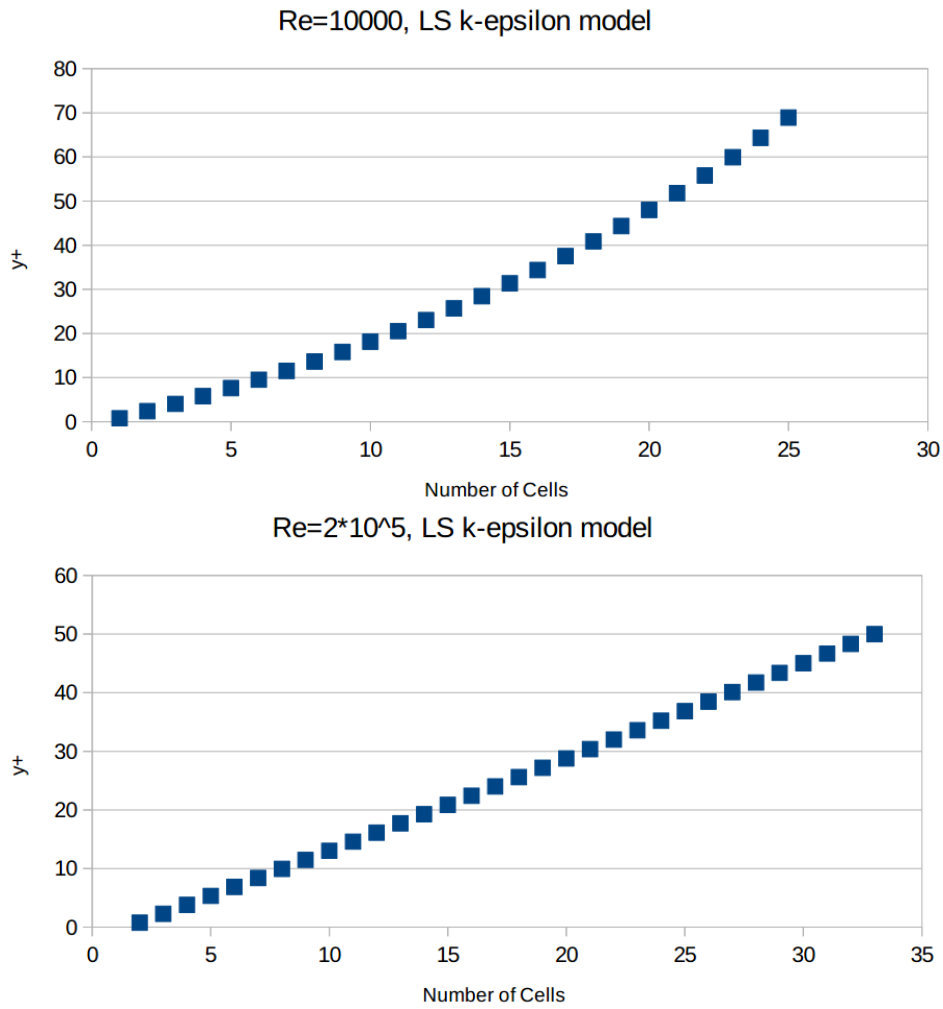

Figure 3.8. Number of Cells within Boundary Layer

Another important thing that should be considered is checking if our grid is mesh independent. Thus, grid convergence study were performed for case with Re=10000. Simulations were performed for 3 different mesh, coarse, medium and fine and Nusselt number were calculated, results can be observed in Figure 3.9.

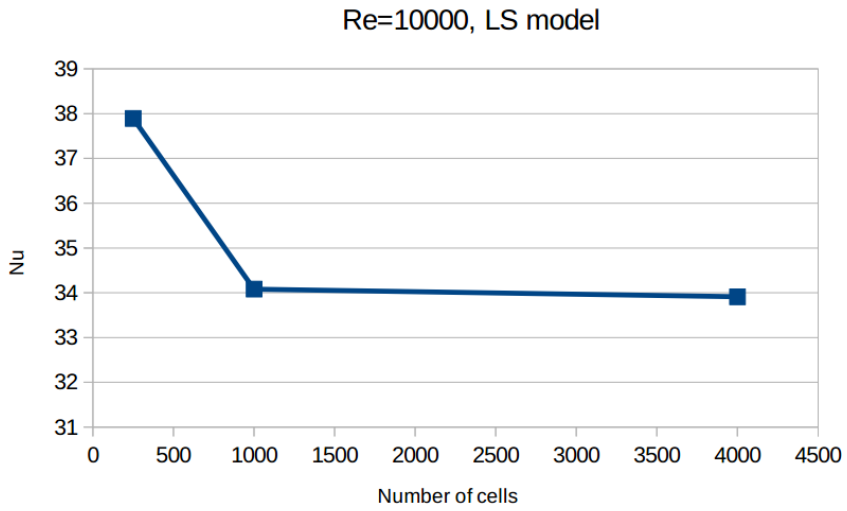

Figure 3.9. Mesh Independence Test

Based on this computations Grid Convergence Index (GCI) and discretization error is estimated [15],

$$GCI = 0.00035 \text{ and } Nu = 33.901 \pm 0.012,$$

which is closer to the value given by Gnielinski for $Re = 10000$ compared with simply coarse mesh value.

CHAPTER 4
LIQUID METAL CORRELATIONS

Liquid metals (LM) have some properties that can be used as an advantage in some processes, they have large thermal conductivity, small kinematic viscosity, small vapor pressure and very wide temperature range over which they remain in liquid phase. Thus, we can say that they are quite efficient environment for heat transfer. They can be used in such processes as power generation from solar energy in concentrated solar panels as a heat transfer fluid. The idea behind concentrated solar panel technology is that the sunlight rays are focused by number of mirrors on a receiver which leads to very high discharge temperatures of a working fluid. Moreover, liquid metals can withstand very high thermal loads, which is another advantage.

In literature there are available many correlations describing the heat transfer but the ones for liquid metals differ significantly from usual ones. Here, in present part of the project liquid metals with fully-developed, forced-convective heat transfer were analyzed. Liquid metals have very low Pr number meaning that thermal boundary layer is much thicker than hydrodynamic one.

Thanks to a dimensional analysis it can be figured out that Nu number has a functional dependence on Re and Pr numbers, however many authors agree that Nu number can be represented by only Peclet number. According to [8] there are few correlations that describe well the dependence of Nu number and Pe, and the best one is Skupinsky correlation, although there are correlations that model particular LM, and they perform better than Skupinsky. All LMs models have following form:

$$Nu = a + bPe^{c}Pr^{d}$$

Where a, b, c, d are constants representing different correlations. They are determined from experimental points, where a uniform heat flux for a pipe was applied by

means of electric heating. The data of the experiments have up to 50% deviations from correlation results for different conducted experiments and the cause of that can be:

- Different experimental setup conditions. Different and improper wetting, or presence of entrained gas can cause large deviations.
- Evaluation of measured data. The values of Nusselt number and Peclet are computed from measured data of temperature, fluid properties, heat flux and flow rates, which combined all together can lead to unsimilar results.
- Problems related with mixed convection. Buoyancy can play huge role, especially in liquid metals.

Launder Shaurma k-epsilon turbulence model were used in order to describe the fluid flow of LMs and the results were compared with Skupinsky correlation and Chen and Chiou, which seems to have best performance, correlation coefficient [8] are shown in Table 4.1. Prandtl number range for LMs analyzed here is from 0.007 to 0.046 where 0.007 corresponds to Sodium Potassium (NaK) fluid, 0.025 corresponds to Lead-Bismuth Eutectic (LBE) and 0.046 corresponds to Mercury (Hg). Results together with bar charts of relative errors for Re number dependence can be observed in Figure 4.1.

Table 4.1. Liquid metal correlations coefficients

	Skupinski	*Chen & Chiou*
a	4.82	5.6
b	0.0185	0.0165
c	0.827	0.85
d	0	0.01

a)

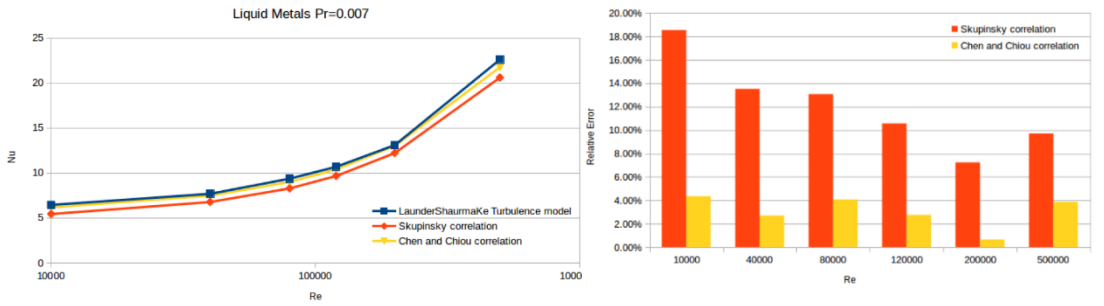

b)

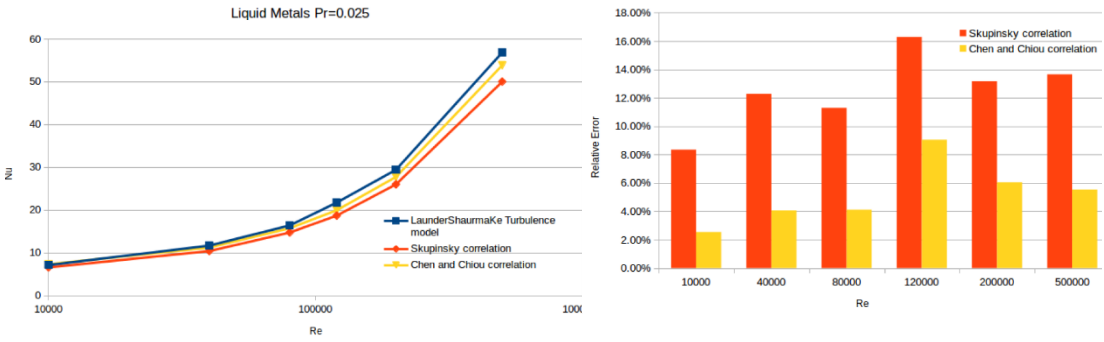

c)

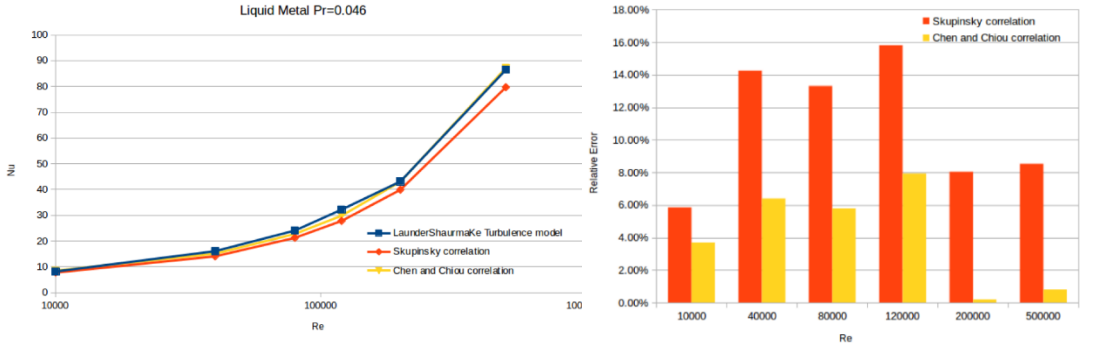

Figure 4.1. Liquid metal correlations and Errors

It can be noticed that Chen and Chiou correlation gives better results (relative errors are lower than in Skupinsky correlation for all Prandtl numbers) if compared with Launder-Shaurma turbulence model.

If we consider that Nu number of LM is function of Pe number only, although we can see that in Chen and Chiou correlation there is a small separate dependence from Pr number (d=0.01), but this small dependence causes very small effect, then the outcome can be viewed in Figure 4.2.

Peclet number is a nondimensional number describing the ratio between advective and diffusive transport rates. Mathematically speaking:

$$Pe = \frac{Advective\ Transport\ Rate}{Diffusive\ Transport\ Rate} = Re_D Pr$$

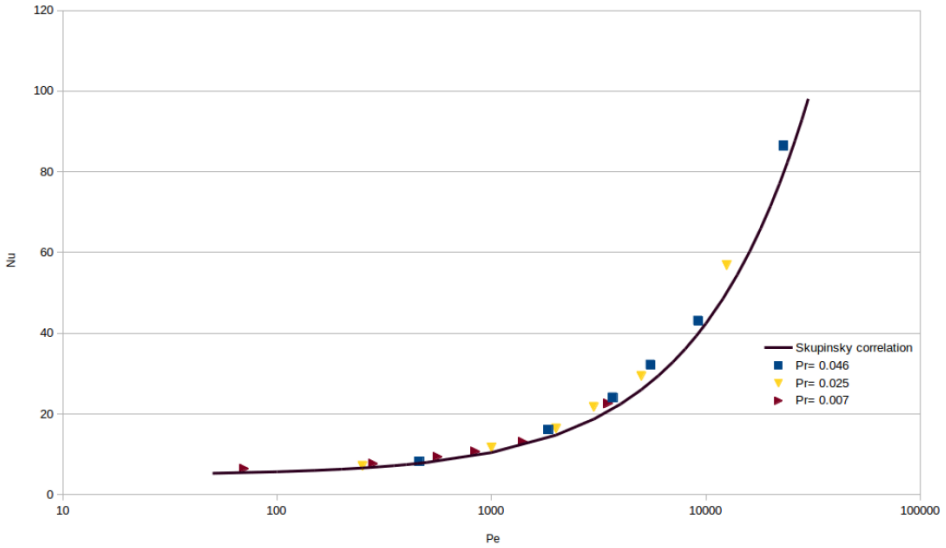

Figure 4.2. Peclet and Nusselt numbers relationship

We can establish that Nusselt number for liquid metals could quite well be described by only one single nondimensional Peclet number according to Figure 4.2.

CHAPTER 5
ENTROPY GENERATION ANALYSIS

Entropy generation minimization is an important topic, it allows us to understand if system behaves in its best performance. Knowing the entropy generation field will allow us to understand where the highest irreversibilities occurs, thus allowing us to assess and optimize problematic areas of geometry. In case of concentrated solar panels receiver tubes we can optimize the diameter based on the optimal Reynolds number. Furthermore, we can comprehend which fluid performs better, minimizing the generated entropy. All of this small improvements can lead to increased performance of the whole solar power plant.

5.1 Mathematical model and solver

Mathematical model is a description of the system using mathematical concepts, in our particular case it will be differential equations. For our investigations and calculations OpenFoam open source toolbox is going to be used since it allows to develop and customize numerical solvers, post-processing and pre-processing utilities for the solution of continuum problems. We are going to implement direct method of entropy generation calculation, thus entropy production will be computed as post-processing value. In order to find velocity and pressure fields RANS equations will be solved, for temperature field simplified energy equation will be applied.

Navier Stokes equation in OpenFoam has following form:

Mathematical Formulation:

$$\frac{\partial}{\partial t}(\rho U) + \nabla \cdot (\phi U) - \mu \nabla^2 U = -\nabla p$$

OpenFoam Formulation:

```
solve
(
      fvm :: ddt(rho, U)
    + fvm :: div(phi, U)
    - fvm :: laplacian(mu, U)
  ==
    - fvc :: grad(p)
);
```

Continuity Equation in OpenFoam:

Mathematical Formulation:

$$\frac{\partial \rho}{\partial t} + \nabla(\rho U) = 0$$

OpenFoam Formulation:

```
solve
(
      fvm :: ddt(rho)
    + fvc :: div(phi)
);
```

As previously mentioned energy equation will be simplified to suit for our case. Full form of energy equation have the following form:

$$\overbrace{\rho c_p \frac{\partial T}{\partial t}}^{\text{I}} + \overbrace{\rho c_p U_i \frac{\partial T}{\partial x_i}}^{\text{II}} = \overbrace{-P \frac{\partial U_i}{\partial x_i}}^{\text{III}} + \overbrace{\lambda \frac{\partial^2 T}{\partial x_i^2}}^{\text{IV}} - \overbrace{\tau_{ij} \frac{\partial U_j}{\partial x_i}}^{\text{V}}$$

Where:

I : Local energy change with time

II : Convection term

III : Pressure work

IV : Heat Diffusion or Heat Flux

V : Irreversible change of mechanical energy into the heat

For our particular case we can use reduced version of energy equation, which is going to perform faster giving us required temperature field. It will suit our case and reasonable simplifications won't cause big deviations from real solution. The simplified energy equation together with turbulence model will have following form:

$$\frac{\partial T}{\partial t} + \vec{u}\nabla T = (\alpha + \alpha_t)\nabla^2 T$$

This equation can be reduced further, since we are interested on steady state solution and we have constant heat flux boundary condition at walls of pipe, moreover, bulk flow is in x direction, so other velocity components are negligible.

$$u\frac{\partial T}{\partial x} = (\alpha + \alpha_t)\left(\frac{\partial^2 T}{\partial y^2} + \frac{\partial^2 T}{\partial x^2}\right)$$

$$\frac{\partial T}{\partial x} = \frac{\partial T_w}{\partial x} = \frac{\partial T_b}{\partial x} = const \rightarrow \frac{\partial^2 T}{\partial x^2} = 0$$

Furthermore, we can divide temperature component into constant value and linear increased value due to constant heat flux at wall.

$$T = \bar{T} + \frac{\partial T}{\partial x}x = \bar{T} + \frac{\Delta T}{L}x$$

where $\frac{\Delta T}{L}$ is a linear growth of temperature along the pipe length.

$$u\overbrace{\frac{\partial \bar{T}}{\partial x}}^{=0} + u\frac{\Delta T}{L} = (\alpha + \alpha_t)\frac{\partial^2 \bar{T}}{\partial y^2}$$

$$0 = (\alpha + \alpha_t)\frac{\partial^2 \bar{T}}{\partial y^2} - u\frac{\Delta T}{L}$$

Temperature field computed with this equation is not suitable for entropy generation calculation, although it correctly represents temperature gradients. Thus, in this case we need absolute temperature field, which will be called as corrected temperature (T_{corr}). This two fields will differ by only a constant value calculated as follows:

$$mc_p T_b = \int_A \rho c_p u \cdot T dA = \int_A \rho c_p \bar{T} dA + \int_A \rho u c_p C dA$$

$$mc_p = \int_A \rho u c_p dA$$

$$T_b = \frac{\int_A \rho c_p \bar{T} dA}{\int_A \rho u c_p dA} + C$$

$$C = T_b - \frac{\int_A \rho c_p \bar{T} dA}{\int_A \rho u c_p dA} \rightarrow T_{corr} = \bar{T} - C$$

By setting bulk temperature to a certain value, in our case it will be 300K, the "C" constant will allow us to reach to the absolute temperature needed in entropy generation equations.

Energy Equation in OpenFoam:

Mathematical Formulation:

$$\mathbf{0} = (\boldsymbol{\alpha} + \boldsymbol{\alpha_t})\frac{\partial^2 \bar{T}}{\partial y^2} - \boldsymbol{u}\frac{\boldsymbol{\Delta T}}{\boldsymbol{L}}$$

OpenFoam Formulation:

```
TEqn(
            fvm::div(phi, T)
          -
fvm::laplacian(alphaEff, T)
          ==
            - mag(U)*gradT
    );
```

In CFD numerical schemes are applied to solve the bunch of differential equations. For each term in partial differential equations different sets of schemes are applied. Table 5.1 summarizes the scheme types used in our cases [16].

Table 5.1. Numerical Schemes

Categories	**Schemes**
Gradient ∇	Gauss linear
Divergence $\nabla \cdot$	Bounded Gauss linear Upwind
Laplacian ∇^2	Gauss linear corrected
Gradient Normal to the cell centre	Corrected
Cell to face interpolation of values	Linear

Gauss linear is a standard finite volume discretization of Gaussian integration where it is required the interpolation of values from cell centers to face centers with linear interpolation scheme.

The advantages of Bounded Gauss linear upwind scheme for divergence calculation was already highlighted above but being short we can say that boundedness is preserved with this scheme leading to better convergence.

Although the orthogonality of the mesh is good for our geometry the corrected scheme for surface normal gradient is used, it adds an explicit non-orthogonal correction to the orthogonal component, thus, maintaining second order accuracy.

The laplacian term scheme is basically the summarization of two schemes cited above, Gauss linear and Corrected.

Interpolation schemes are used to interpolate values from cell centers to face cell centers. Primarily it is used to interpolate velocities to face centers for the calculation of flux ϕ.

In OpenFoam there are different available linear solvers to solve discretized differential equations. Pressure equation uses Preconditioned Bi-Conjugate Gradient (PBiCG) solver with Diagonal incomplete LU (DILU) preconditioner. Momentum, turbulent and energy equations use smooth solvers with Gauss-Seidel smoother, which generally is the most reliable and robust option providing good convergence.

In order to be able to compute new fields of entropy produced the OpenFoam library **swak4foam** is going to be used. It combines the functionality of **groovyBC** [9] and **funkySetFields** [10] by offering the possibility to specify the expressions involving the fields and evaluate them, thus allowing to do many things avoiding programming.

Following entropy generation equations, previously derived, are going to be used and their swak4foam formats are shown in Table 5.2.

Table 5.2. Swak4foam formulations

Mathematical Formulation:	*OpenFoam **swak4foam** Formulation:*

$S_{gen,fric,mean} = \frac{\mu}{\bar{T}}\left[2\left\{\left(\frac{\partial \bar{u}}{\partial x}\right)^2 + \left(\frac{\partial \bar{v}}{\partial y}\right)^2 + \left(\frac{\partial \bar{w}}{\partial z}\right)^2\right\} + \left(\frac{\partial \bar{u}}{\partial y} + \frac{\partial \bar{v}}{\partial x}\right)^2 + \left(\frac{\partial \bar{u}}{\partial z} + \frac{\partial \bar{w}}{\partial x}\right)^2 + \left(\frac{\partial \bar{v}}{\partial z} + \frac{\partial \bar{w}}{\partial y}\right)^2\right]$	SgenFricMeanExpression
	{
	field SgenFricMeanPost;
	variables "nu=0.00001;";
	expression
	"nu*2*magSqr(symm(grad(U)))/Tcorr";
	dimension [0 2 -3 -1 0 0 0];
	create true;
	}

$S_{gen,heat,mean} = \frac{\lambda}{\bar{T}^2}\left[\left(\frac{\partial \bar{T}}{\partial x}\right)^2 + \left(\frac{\partial \bar{T}}{\partial x}\right)^2 + \left(\frac{\partial \bar{T}}{\partial x}\right)^2\right]$	SgenHeatMeanExpression
	{
	field SgenHeatMeanPost;
	variables
	"Pr=0.007;nu=0.00001;lambda=nu/Pr;";
	expression
	"lambda/sqr(Tcorr)*magSqr(grad(Tcorr))";
	dimension [0 2 -3 -1 0 0 0];
	create true;
	}

$S_{gen,fric,fluc} = \frac{\rho\epsilon}{\bar{T}}$	SgenFricFluctExpression
	{
	field SgenFricFluctPost;
	expression **"epsilon/Tcorr"**;
	dimension [0 2 -3 -1 0 0 0];
	create true;
	}

$S_{gen,heat,fluc} = \frac{\alpha_t}{\alpha} S_{gen,heat,mean}$	SgenHeatFluctExpression
	{
	field SgenHeatFluctPost;
	variables
	"Pr=0.007;Prt=0.85;nu=0.00001;";
	expression
	"nut/nu*Pr/Prt*SgenHeatMeanPost";
	dimension [0 2 -3 -1 0 0 0];
	create true;
	}

To be able to understand why entropy generation S_{gen} have this OpenFoam forms let's look into subsequent equations [11]:

$$grad(\vec{U}) = \begin{bmatrix} \frac{\partial U_x}{\partial x} & \frac{\partial U_x}{\partial y} & \frac{\partial U_x}{\partial z} \\ \frac{\partial U_y}{\partial x} & \frac{\partial U_y}{\partial y} & \frac{\partial U_y}{\partial z} \\ \frac{\partial U_z}{\partial x} & \frac{\partial U_z}{\partial y} & \frac{\partial U_z}{\partial z} \end{bmatrix}$$

$$symm(grad(\vec{U})) = \frac{1}{2}\begin{bmatrix} 2\frac{\partial U_x}{\partial x} & \frac{\partial U_x}{\partial y} + \frac{\partial U_y}{\partial x} & \frac{\partial U_x}{\partial z} + \frac{\partial U_z}{\partial x} \\ \frac{\partial U_y}{\partial x} + \frac{\partial U_x}{\partial y} & 2\frac{\partial U_y}{\partial y} & \frac{\partial U_y}{\partial z} + \frac{\partial U_z}{\partial y} \\ \frac{\partial U_z}{\partial x} + \frac{\partial U_x}{\partial z} & \frac{\partial U_z}{\partial y} + \frac{\partial U_y}{\partial z} & 2\frac{\partial U_z}{\partial z} \end{bmatrix}$$

$$magSqr\left(symm\left(grad(\vec{U})\right)\right) =$$

$$= \left(\frac{\partial U_x}{\partial x}\right)^2 + \left(\frac{\partial U_y}{\partial y}\right)^2 + \left(\frac{\partial U_z}{\partial z}\right)^2 + 0.5\left(\frac{\partial U_x}{\partial y} + \frac{\partial U_y}{\partial x}\right)^2 + 0.5\left(\frac{\partial U_y}{\partial z} + \frac{\partial U_z}{\partial y}\right)^2$$

$$+ 0.5\left(\frac{\partial U_x}{\partial z} + \frac{\partial U_z}{\partial x}\right)^2$$

Note: In OpenFoam

$$mag(T) = sqrt(T{:}T)$$

$$magSqrt(T) = T{:}T$$

where ":" means double inner product [17].

$$ex{:}\quad T{:}S = T_{11}S_{11} + T_{12}S_{12} + T_{13}S_{13} + \cdots$$

5.2 Meshing and Boundary Conditions

Meshing or in other words discretization is a process of splitting big geometries into smaller fragments. This small blocks have their own nodes and boundary faces. In finite volume method all differential equations are applied to it and later are reduced to algebraic equations to be solved with computer. In our case the geometry is simple pipe and it can be discretized into smaller fragments which will be small rectangle, this kind of mesh is called structural mesh, and it has many advantages previously mentioned. Knowing that pipe have symmetry plane we can reduce the amount of mesh by twice by just assigning symmetry boundary condition. Sometimes it can be deceptive, geometries seeming to have ideal symmetry line may not have symmetry in flow field, and as an example we can give an external flow of fluid over the cylinder. Geometry seems to be in symmetry but due to Von Karman vortexes [18] fluid flow is not symmetrical, moreover they don't have steady state solution, Figure 5.1. In case of internal flow inside the pipe there is no such vortexes and fluid flow field can be considered as symmetrical, Figure 5.2.

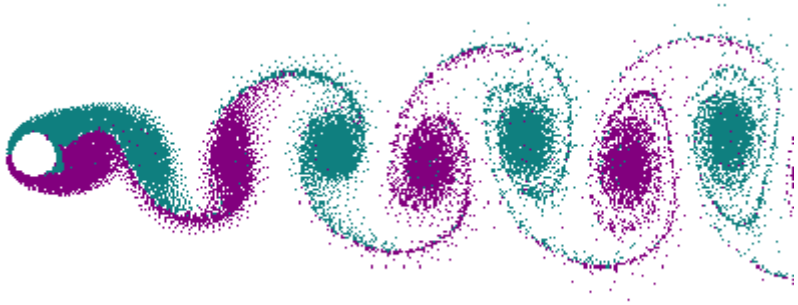

Figure 5.1. Nonsymetrical vortexes

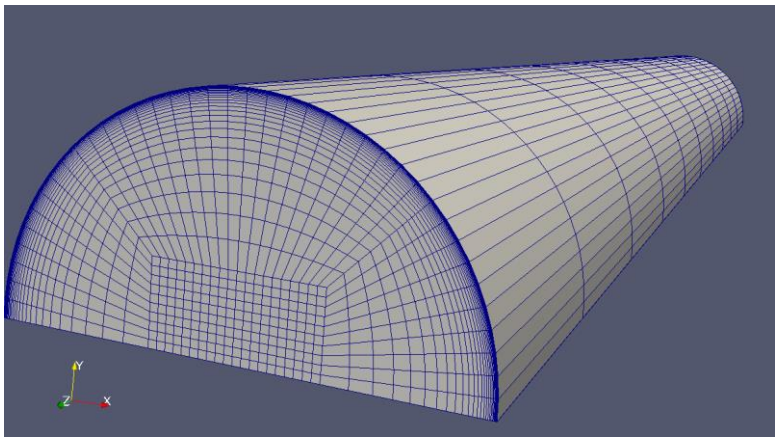

Figure 5.2. Mesh for symetrical fluid flow

As said above, we have bunch of differential equations. It is known that differential equations have unlimited possible solutions unless proper boundary conditions are applied. At the inlet and the outlet of the pipe cyclic boundary conditions are applied. This kind of boundary condition allows us to achieve fully developed flow inside pipe with relatively short pipe geometry length. Turbulent kinetic energy and turbulent dissipation rate for inlet boundary condition and as a field initialization can be calculated using turbulence intensity(I) property [19], which for medium turbulence can take 5% value, or can be calculated based on Re number of flow.

$$I = 0.16(Re)^{-\frac{1}{8}}$$

$$k_{in} = \frac{3}{2}(IU)^2$$

$$\epsilon_{in} = \frac{C_\mu^{0.75} k^{\frac{3}{2}}}{l}; \quad where\ l = 0.07D\ and\ is\ called\ turbulent\ length\ scale.$$

Paramount importance carry boundary condition at a wall related with energy equation. For uniform heat flux Neuman boundary condition are going to be applied, meaning that the temperature gradient should be assigned there. In order to understand what values have to take the temperature gradients at the wall we should do the following for constant heat flux at the wall:

$$\left(\frac{\partial T}{\partial n}\right)_w = \frac{q_w}{\lambda} = \frac{mc_p\Delta T}{\lambda\pi DL} = \frac{mc_p\frac{\Delta T}{L}}{\lambda\pi D} = \frac{\rho u_b\frac{\pi D^2}{4}c_p\frac{\Delta T}{L}}{\lambda\pi D} = \frac{1}{4}\frac{\rho u_b D}{\mu}\frac{c_p\frac{\Delta T}{L}}{\lambda}$$

$$\left(\frac{\partial T}{\partial n}\right)_w = \frac{1}{4}Re_b\mathrm{Pr}\frac{\Delta \mathrm{T}}{L}$$

Since $\frac{dT_b}{dx} = \frac{\partial T}{\partial x} = const = \frac{\Delta \mathrm{T}}{L}$ and $q" = const$ temperature gradient value at the wall becomes function of Reynolds and Prandtl numbers.

In case of non-uniform heat flux boundary condition at the wall will slightly differ. Half of the wall will be considered adiabatic, meaning that $\left(\frac{\partial T}{\partial n}\right)_w = 0$, in another half cosinusoidal heat flux will be applied representing the density of solar rays concentration[12], Figure 5.3.

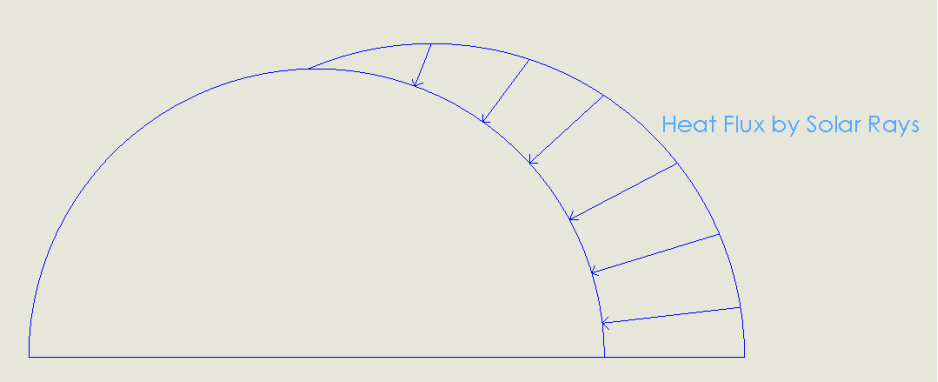

Figure 5.3. Cosinusoidal heat flux

Thus for OpenFoam the cosinusoidal heat flux can be represented as follows:

$$Q' = mc_p \frac{\Delta T}{L} = \int_0^{\frac{\pi}{2}} \overline{q"} cos(\theta) \frac{D}{2} d\theta$$

$$\overline{q"} = \frac{2mc_p \frac{\Delta T}{L}}{D} \cdot \frac{4\pi\mu}{4\pi\mu} = \frac{Re\mu c_p \pi \frac{\Delta T}{L}}{4}$$

$$\overline{\left(\frac{\partial T}{\partial n}\right)_w} = \frac{1}{4} Re_b \mathrm{Pr}\, \pi \frac{\Delta \mathrm{T}}{L}$$

Thus the wall boundary condition will have the subsequent form:

$$\overline{\left(\frac{\partial T}{\partial n}\right)_w} = \frac{1}{4} Re_b \mathrm{Pr}\, \pi \frac{\Delta \mathrm{T}}{L} \cdot \cos(\theta)$$

where θ can be described with geometrical parameters for each cell face located at wall boundary.

Here we can understand that the temperature gradient at wall will change depending on the type of the fluid considered and Reynolds number of the flow for the same amount of heat supply to the domain.

5.3 Analysis of Results

Predicting efficient thermal use in energy systems carries paramount importance, since the amount of available work is dependent on the amount of entropy generated. Therefore, systems with smaller entropy productions leads to lesser irreversibilities, thus, higher available work. So the objective of this part of thesis is understanding how and what leads to lower entropy generation in concentrated solar panels.

In literature there are already available algebraic equations for specific cases of uniform heat flux on the surface of the tube heat exchangers [9]. Those equations together

with numerical results are going to be compared to check the correctness of simulation results.

According to A. Bejan [4] and [13] for constant heat input per unit length ($\dot{Q}'$) and constant mass flow rate ($\dot{m}$) the entropy generation equation is as following:

$$\boldsymbol{S'_{gen} = \frac{Q'^2}{\pi\lambda T^2 Nu} + \frac{32\dot{m}^3 f}{\pi^2 T\rho^2 D^5}}$$

By applying friction factor correlation of McAdams:

$$f = A \cdot Re^{-B}$$

where $A = 0.046\ and\ B = 0.2$,

and Dittus-Boelter correlation:

$$Nu = \alpha Re^{\beta} Pr^{\gamma}$$

where $\gamma = 0.4,\ \ \beta = 0.8,\ \ \alpha = 0.023\ for\ 0.6 < Pr < 160,\ \ and\ \gamma = 0.4,\ \ \beta = 0.4,$

$\alpha = 0.625\ \ for\ 0.005 < Pr < 0.05$

$$S'_{gen} = \frac{Q'^2}{\pi\lambda T^2 \alpha Re^{\beta} Pr^{\gamma}} + \frac{32\dot{m}^3 A \cdot Re^{-B}}{\pi^2 T\rho^2 D^5}$$

In order to find which value of Re number minimizes the generated entropy S'_{gen} equation have to be differentiated by Re and equated to zero.

$$\frac{\partial S'_{gen}}{\partial Re} = -\frac{\beta Q'^2}{\alpha\pi\lambda T^2 Re^{\beta+1}} \cdot Pr^{-\gamma} + \frac{(5-B)A\pi^3\mu^5}{32\rho^2 T\dot{m}'} \cdot Re^{4-B} = 0$$

$$\boldsymbol{Re_{opt} = \left(\frac{(32\beta\dot{m}^2\rho^2 Q'^2)}{(5-B)A\pi\alpha\lambda T\mu^5}\right)^{\frac{1}{5-B+\beta}}}$$

Now, in order to generalize the case, we can normalize the equation based on Re_{opt}.

$$S'_{gen} = \bar{A}Re^{-\beta} + \bar{B}\ Re^{5-B}; \bar{A} = \frac{Q'^2}{\pi\lambda T^2 \alpha Pr^{\gamma}}; \bar{B} = \frac{\pi^3\mu^5 A}{32T\rho^2\dot{m}^2}$$

$$N_s = \frac{S'_{gen}}{S'_{gen,min}} = \frac{\bar{A}Re^{-\beta} + \bar{B}\ Re^{5-B}}{\bar{A}Re_{opt}^{-\beta} + \bar{B}\ Re_{opt}^{5-B}} = \frac{\bar{A}}{\bar{A} + \bar{B}Re_{opt}^{5-B+\beta}} \cdot \left(\frac{Re}{Re_{opt}}\right)^{-\beta} + \frac{\bar{B}}{\bar{A}Re_{opt}^{-\beta-5+B} + \bar{B}} \cdot \left(\frac{Re}{Re_{opt}}\right)^{5-B}$$

$$Re_{opt}^{5-B+\beta} = \frac{\overbrace{32\rho^2\dot{m}^2 T}^{1/\bar{B}}}{\pi^3\mu^5 A} \cdot \frac{\overbrace{Q'^2}^{\bar{A}}}{\alpha\pi\lambda T^3 Pr^{\gamma}} \cdot \frac{\beta}{5-B}$$

$$Re_{opt}^{5-B+\beta} = \bar{A}\bar{B}^{-1} \cdot \frac{\beta}{5-B}$$

$$N_s = \frac{\bar{A}}{\bar{A} + \bar{B}\bar{A}\bar{B}^{-1} \cdot \frac{\beta}{5-B}} \cdot \left(\frac{Re}{Re_{opt}}\right)^{-\beta} + \frac{\bar{B}}{\bar{A}\bar{B}\bar{A}^{-1} \cdot \frac{5-B}{\beta} + \bar{B}} \cdot \left(\frac{Re}{Re_{opt}}\right)^{5-B}$$

$$\boldsymbol{N_s = \frac{1}{1 + \frac{\beta}{5-B}} \cdot \left(\frac{Re}{Re_{opt}}\right)^{-\beta} + \frac{1}{\frac{5-B}{\beta} + 1} \cdot \left(\frac{Re}{Re_{opt}}\right)^{5-B}}$$

Hereafter normalized entropy generation equation will be used to assess the results of simulations.

Figure 5.4 demonstrate the solution fields of velocity and temperature for uniform heat flux, primarily fields that need to be calculated. As it can be observed highest temperature is on the wall boundary where temperature gradient was applied. In order to judge if the fields are converged we can monitor the temperature value inside a random cell, Figure 5.5, realizing that the temperature value is not changing with iterations.

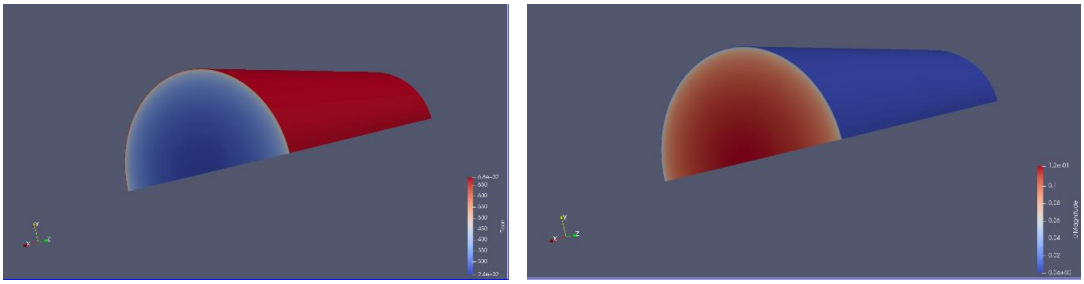

Figure 5.4. Temperature and velocity fields in uniformly heat pipe

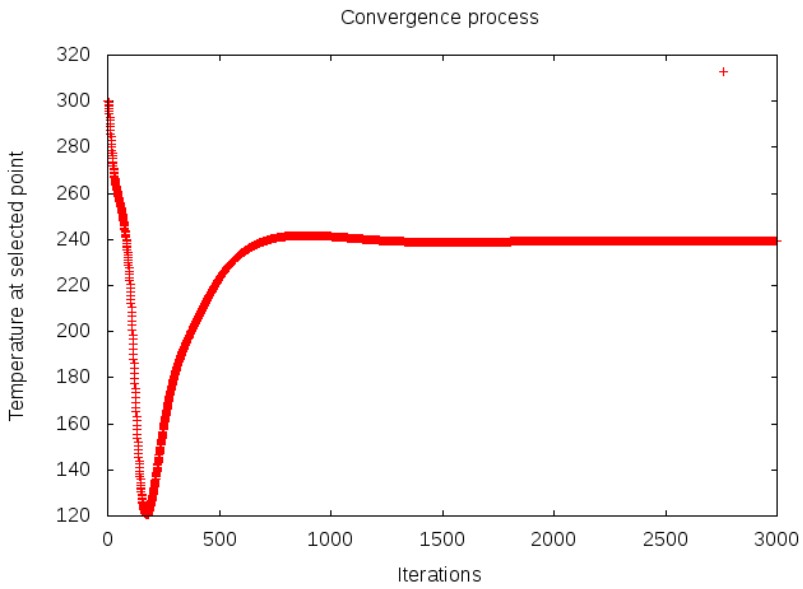

Figure 5.5. Convergence process

Knowing velocity and temperature fields, entropy generation fields can be estimated. Figure 5.6 demonstrates us four entropy production terms. By analyzing this fields we can understand that mean values of entropy production terms have maximum values at the wall. It is expected since at this point gradients are highest. Fluctuating terms have different behavior, at the wall boundary their values are null, but close to wall they have their peak values.

a) Entropy generation due to mean heat transfer

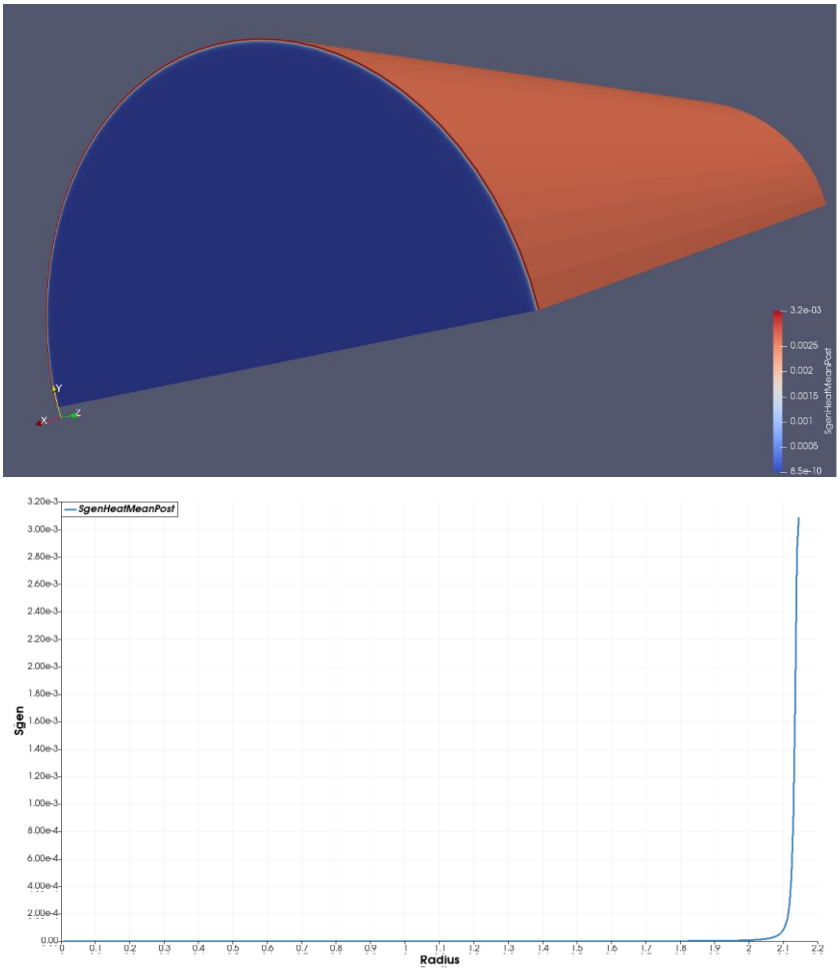

b) Entropy generation due to fluctuating heat transfer

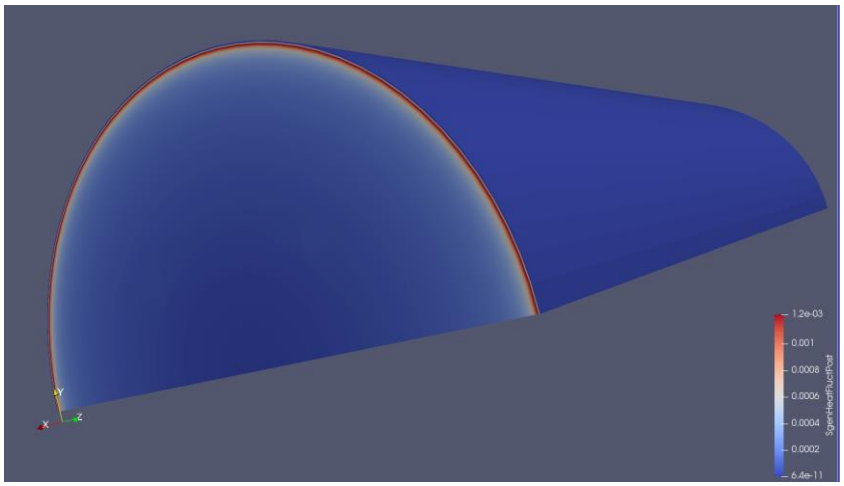

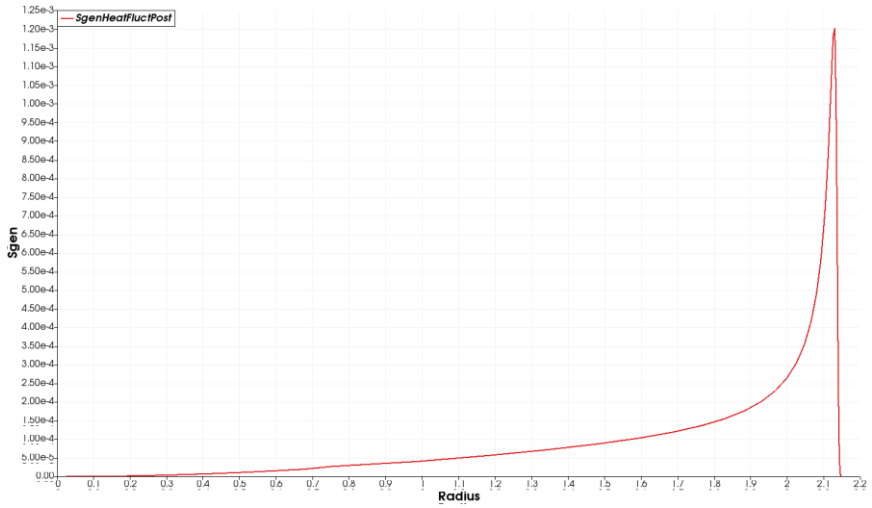

c) *Entropy generation due to mean friction component*

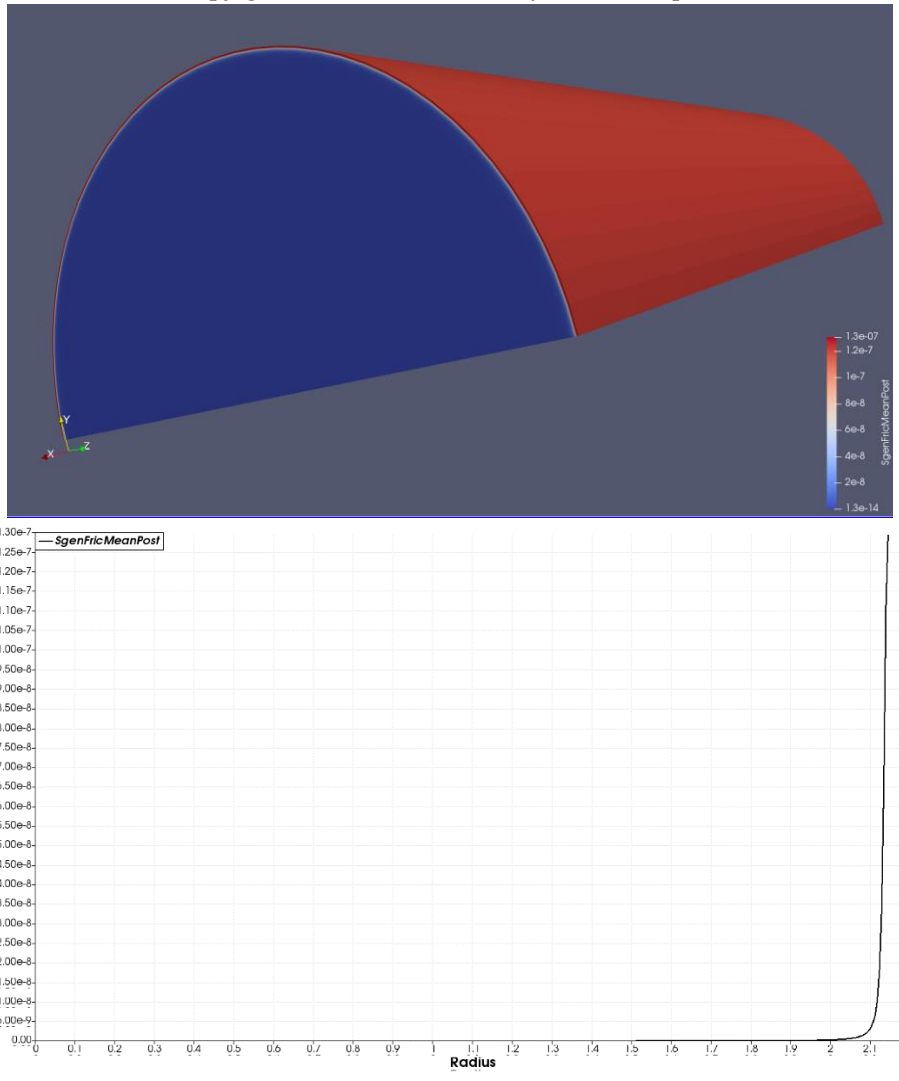

d) Entropy generation due to fluctuating friction component

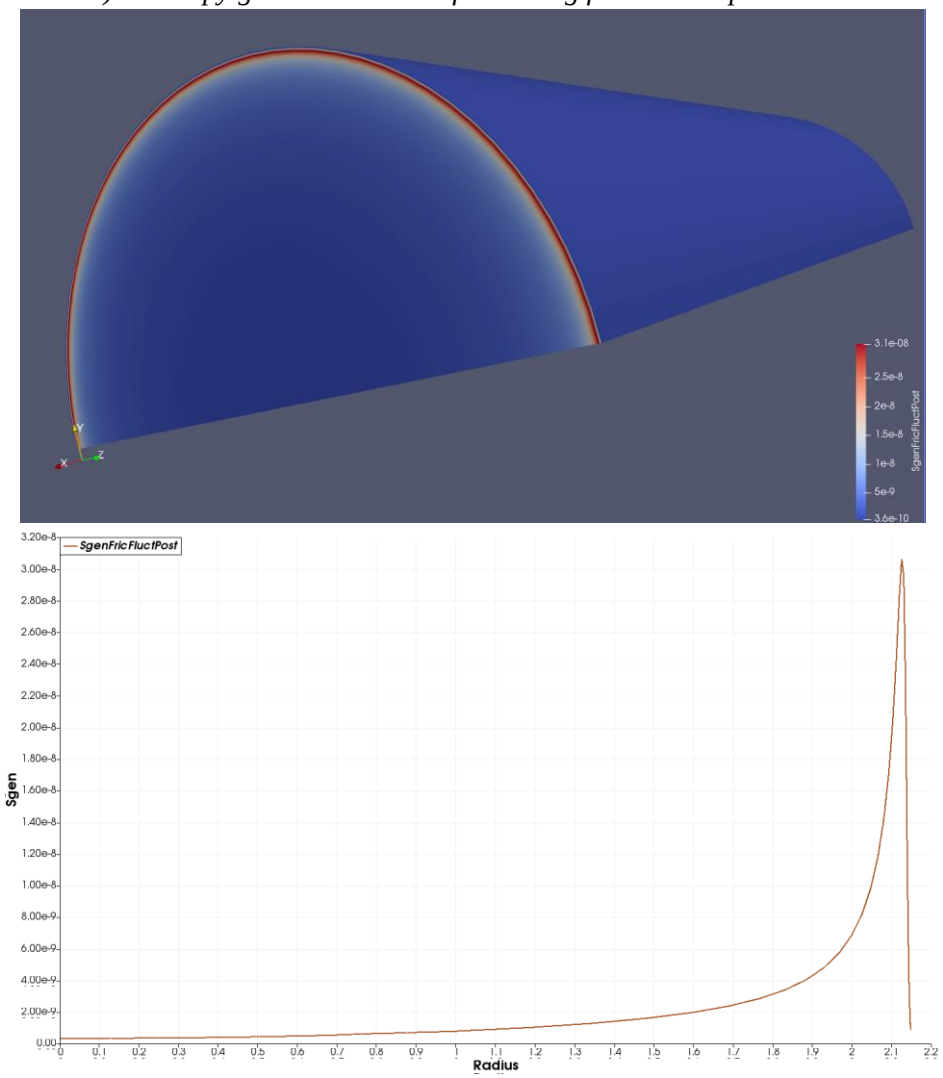

Figure 5.6. Entropy generation fields in uniformly heated duct

Further the results of entropy generation for non-uniform heat flux will be analyzed. Non uniform heat flux case is more realistic for the concentrated solar panels application and it does not have any semi analytical derivation in literature, this is the reason why its simulation results are caring big importance in our research. Figure 5.7 demonstrates the results for non-uniform case, and the difference can be seen from the first glance. Left hand side of the pipe is heated with non-uniform cosinusoidal heat flux. In current case velocity and energy equations are uncoupled, thus the temperature field is not affecting the velocity.

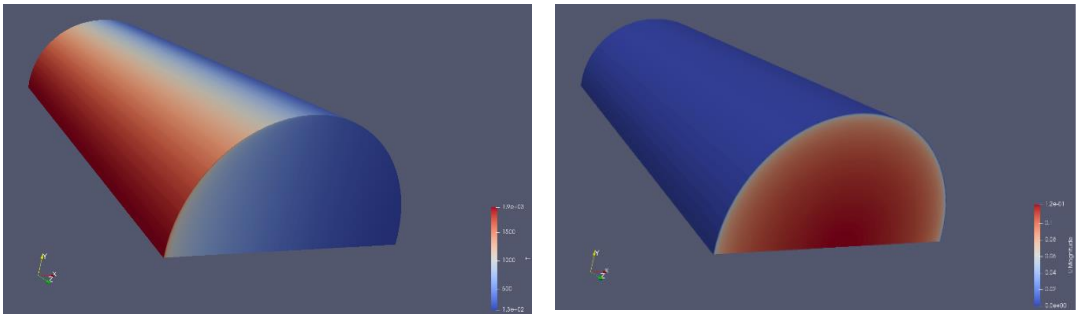

Figure 5.7. Temperature and velocity fields in non-uniformly heated duct

By knowing temperature and velocity fields the entropy generation fields can be computed. Figure 5.8 demonstrates the results.

a) Entropy generation due to mean heat transfer

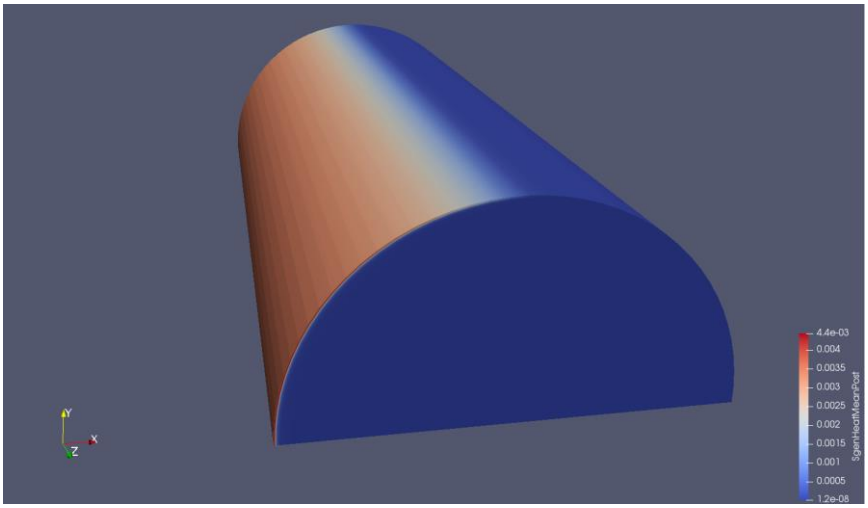

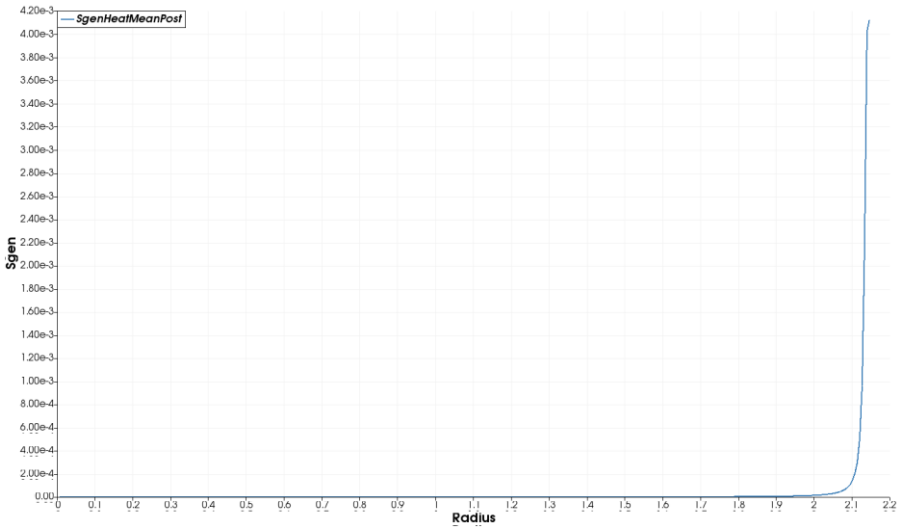

b) Entropy generation due to fluctuating heat transfer

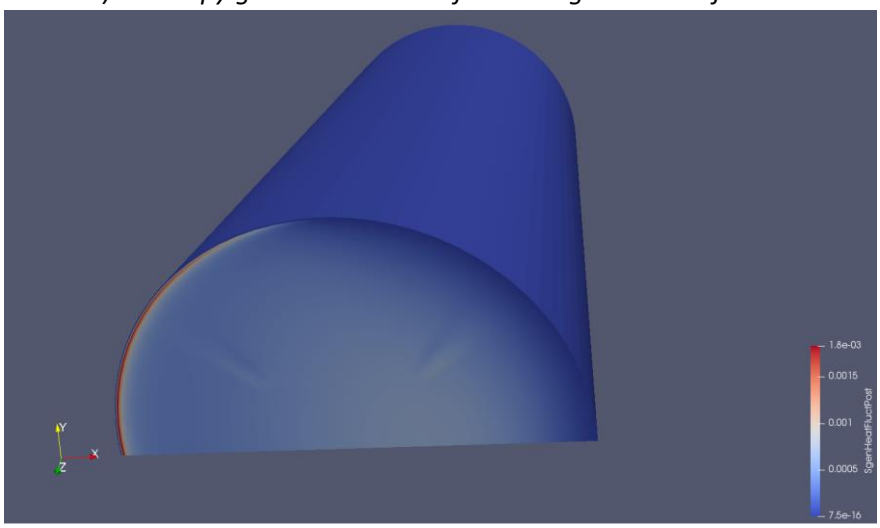

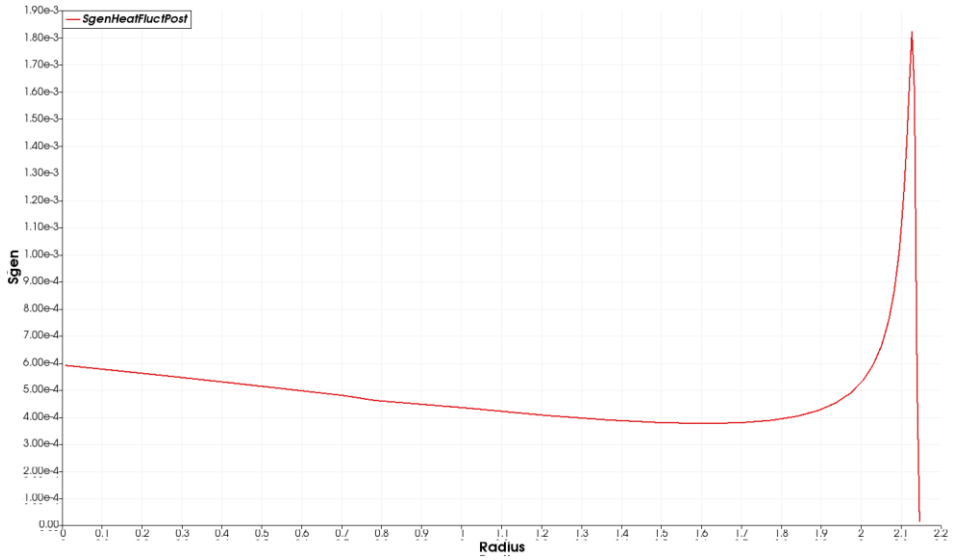

c) *Entropy generation due to mean friction component*

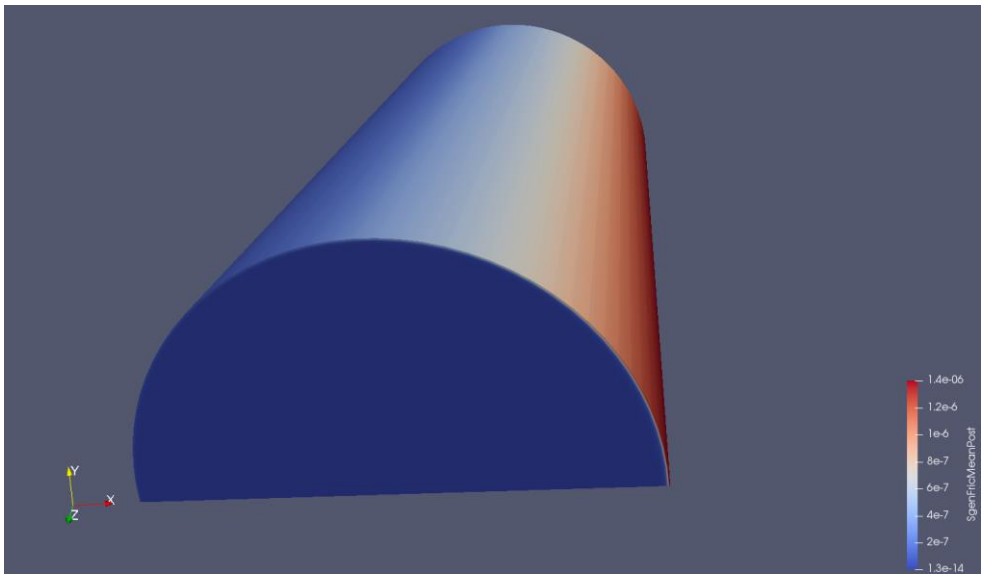

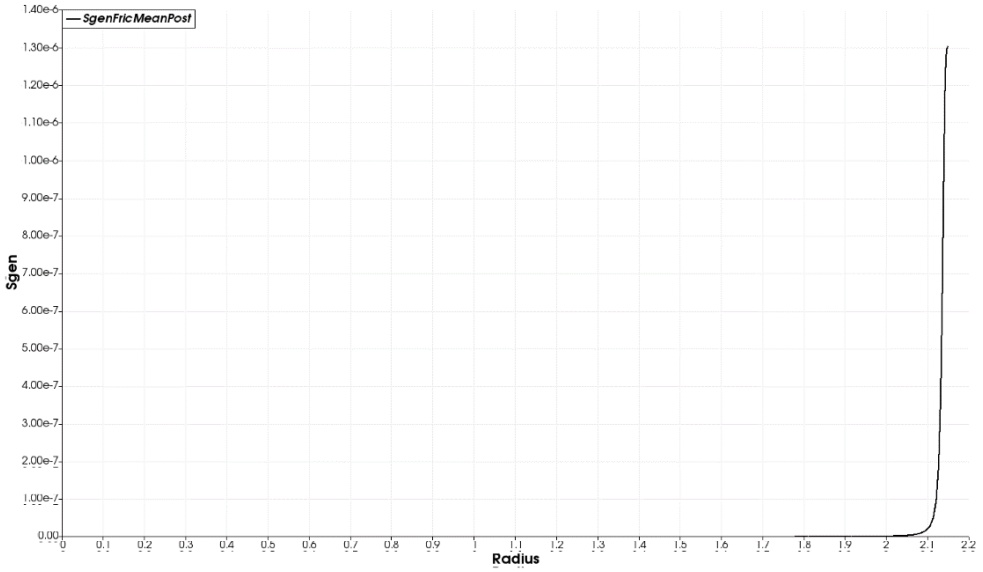

d) Entropy generation due to fluctuating friction component

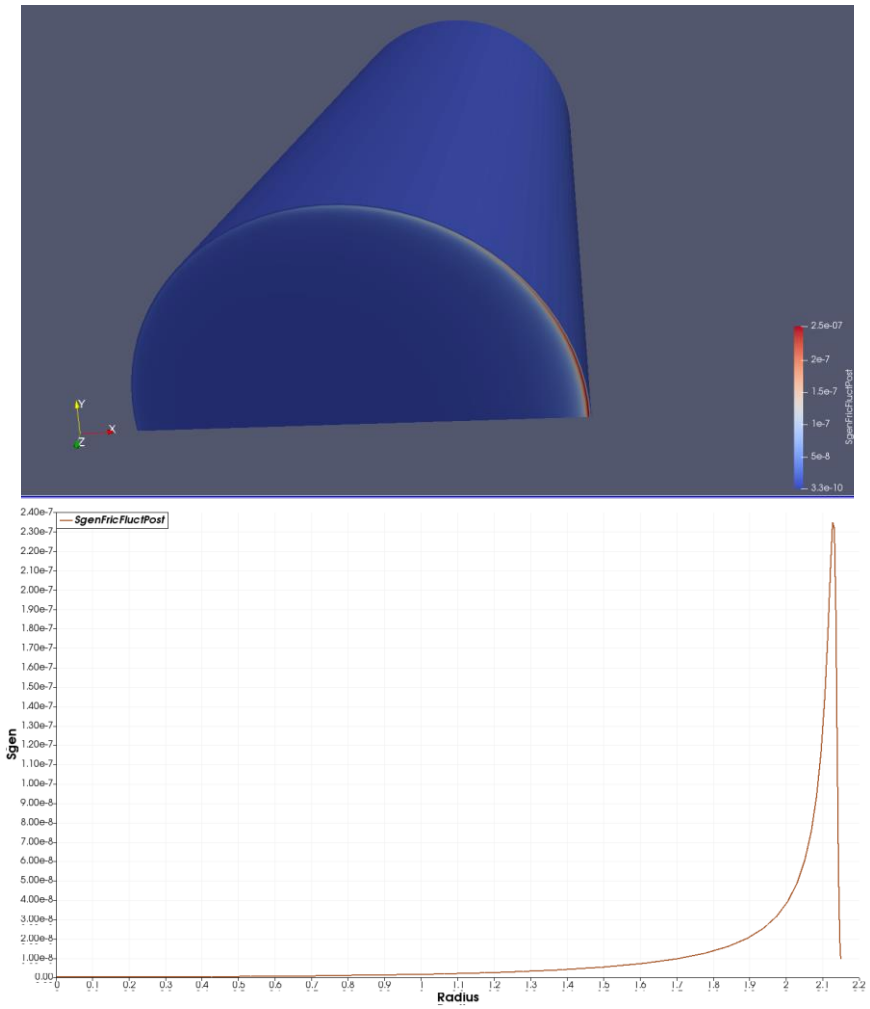

Figure 5.8. Entropy generation fields in non-uniformly heated duct

We can understand that at the wall boundary where the heat flux occurs the entropy generation terms due to friction are lower compared with adiabatic wall since entropy generation is inversely proportional to temperature of the field. Thus we can say that the higher the temperature of the fluid the lower the entropy production. Mean components of the entropy production have their maximum exactly at the wall boundary, while the fluctuating values have their peaks close to the wall.

Entropy generation is dependent on the Reynolds number of the flow and the Prandtl number of the fluid. Figure 5.9 demonstrates us optimal Reynolds numbers for different Prandtl numbers.

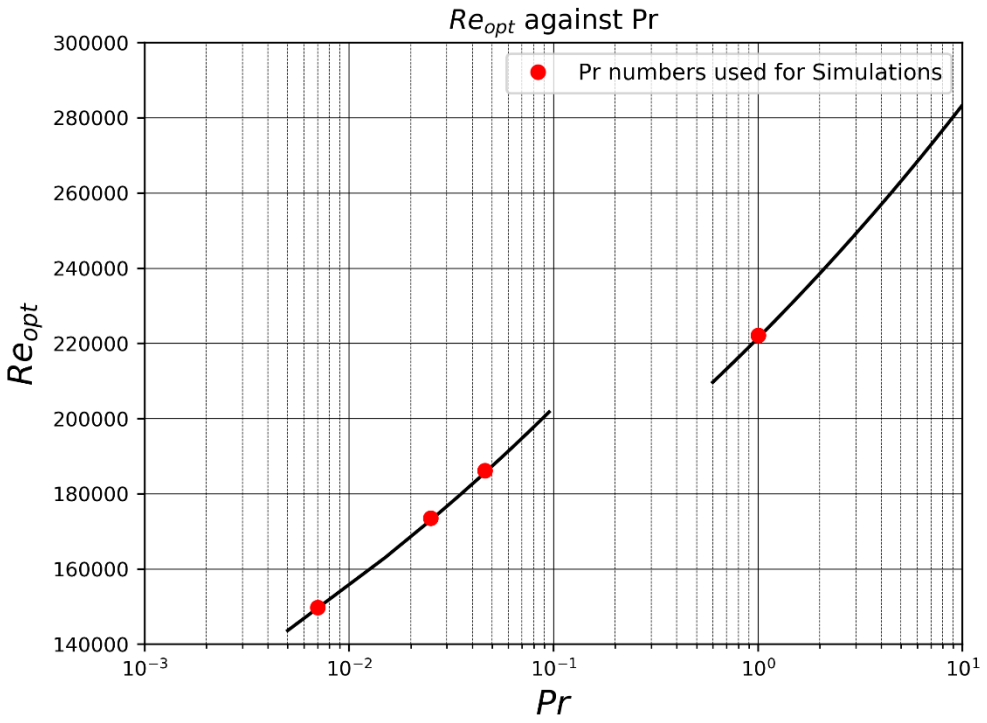

Figure 5.9. Optimal Reynolds number dependency on Pr number

We can observe certain gap in the range $0.1 < Pr < 0.6$, since Nusselt number correlations neither for liquid metals neither for gases covers this region. Using this optimal Reynolds numbers normalized or in other words generalized results for all the cases can be constructed. Moreover, we can use this information to understand what kind of fluid is best suited for given Reynolds number of the flow.

In addition to optimal Reynolds value we can examine the entropy generated at optimal Reynolds numbers. Figure 5.10 illustrates to us that low Prandtl number fluids generates lesser entropy, thus, they are more efficient to use. In addition to it we can notice that at uniform heat flux system are in more order, producing lesser entropy, hence higher exergy of the system.

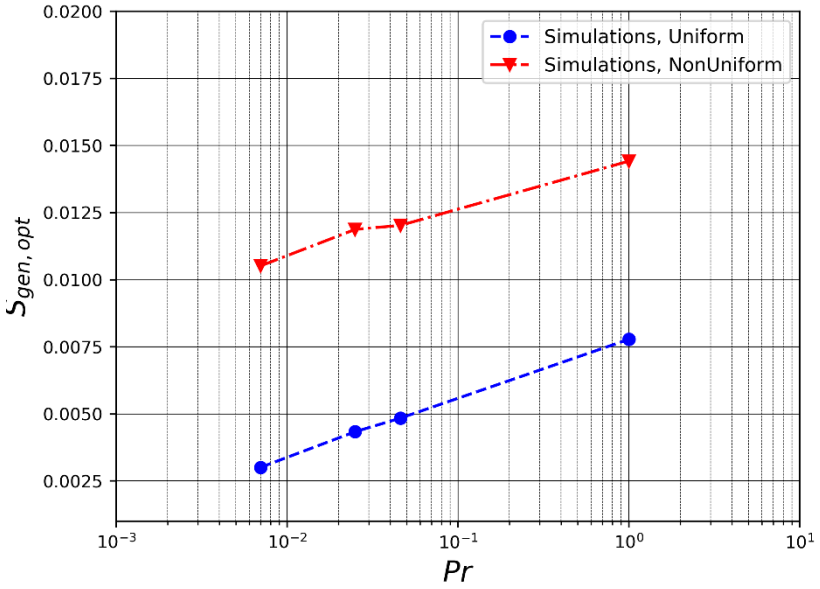

Figure 5.10. Optimum Entropy generation values

In previous chapters nondimensional entropy equation for constant heat flux and mass flow rate were derived. Those results will be compared with simulation for both uniform and non-uniform heat flux cases. Figure 5.11 contains the results for $Pr = 1$.

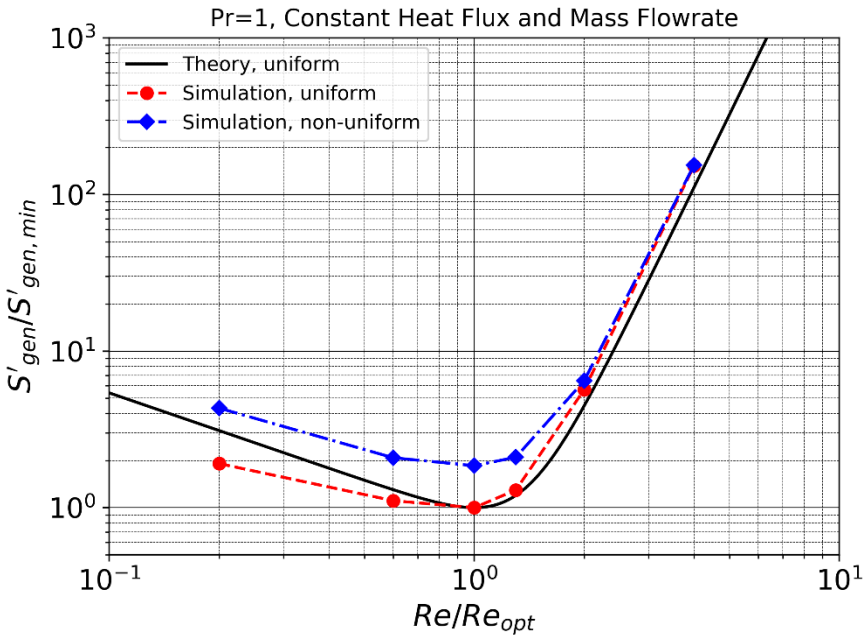

Figure 5.11. Normalized entropy generation, Pr=1

We can observe that for high Re number fluid flows there is quite good agreement. At high Re number flows entropy production due to friction dominates while entropy generation due to heat flux has minor effect, hence we can notice that non-uniform and uniform curves coincide at large Re numbers. As opposite, at low Re number flows entropy generation due to heat flux prevails, thus we can see the difference in behavior of uniformly heated and non-uniformly heated systems. Important point is that there is a minimum point, where the sum of entropy production due to heat transfer and friction has minimum value. We should operate our system as close as possible to that extremum point.

The similar results are obtained for liquid metal fluids, Figure 5.12-5.14.

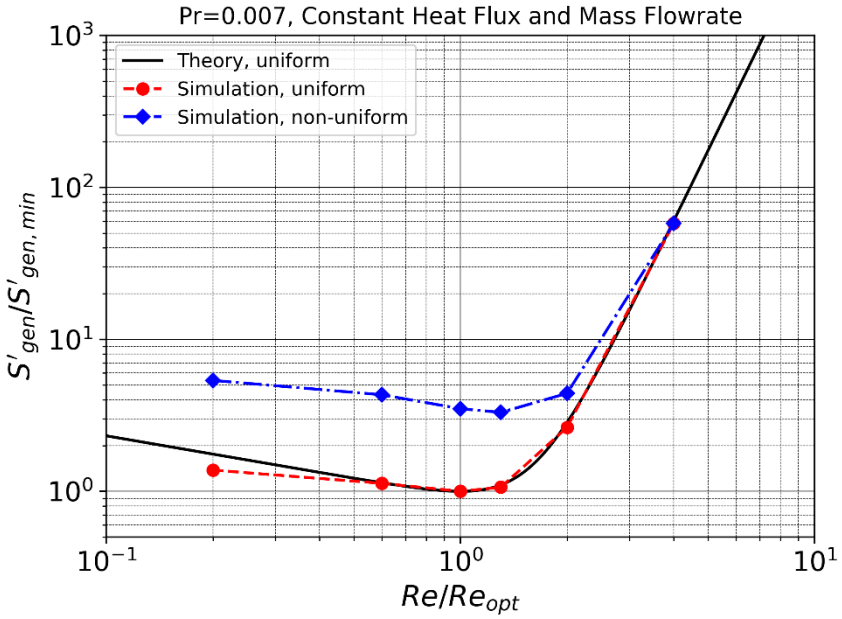

Figure 5.12. Normalized entropy generation, Pr=0.007

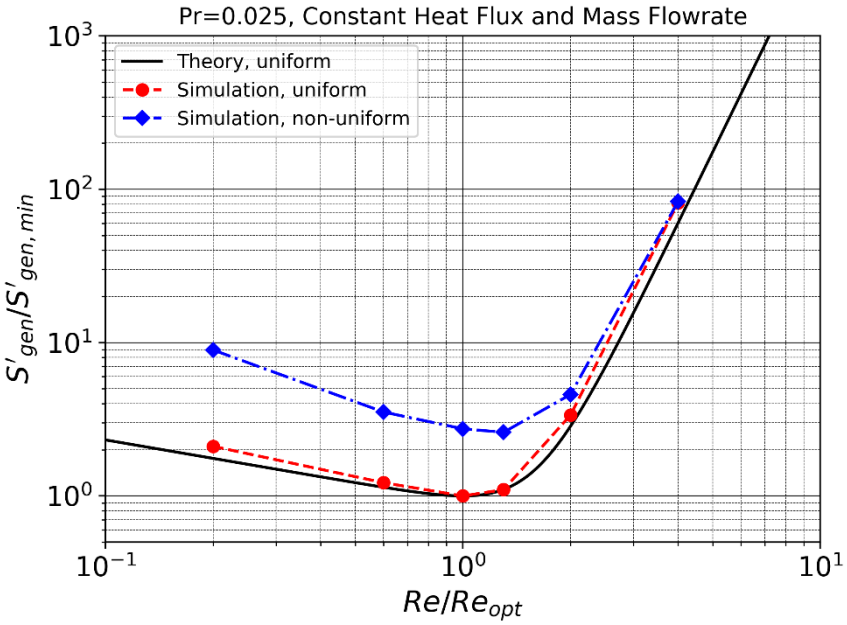

Figure 5.13. Normalized entropy generation, Pr=0.025

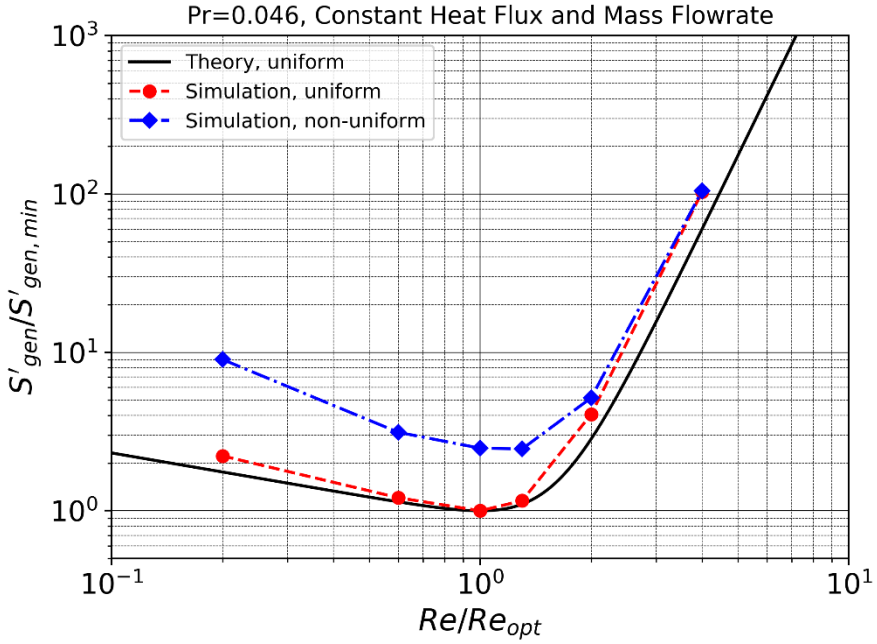

Figure 5.14. Normalized entropy generation, Pr=0.046

Smaller the Prandtl number of the fluid larger the difference between uniform and non-uniform cases, although that difference reduces to zero at large Reynolds numbers.

Sometimes it can be useful to see how each component of entropy production terms changes with Reynolds numbers. Figure 5.15 exposes it to us.

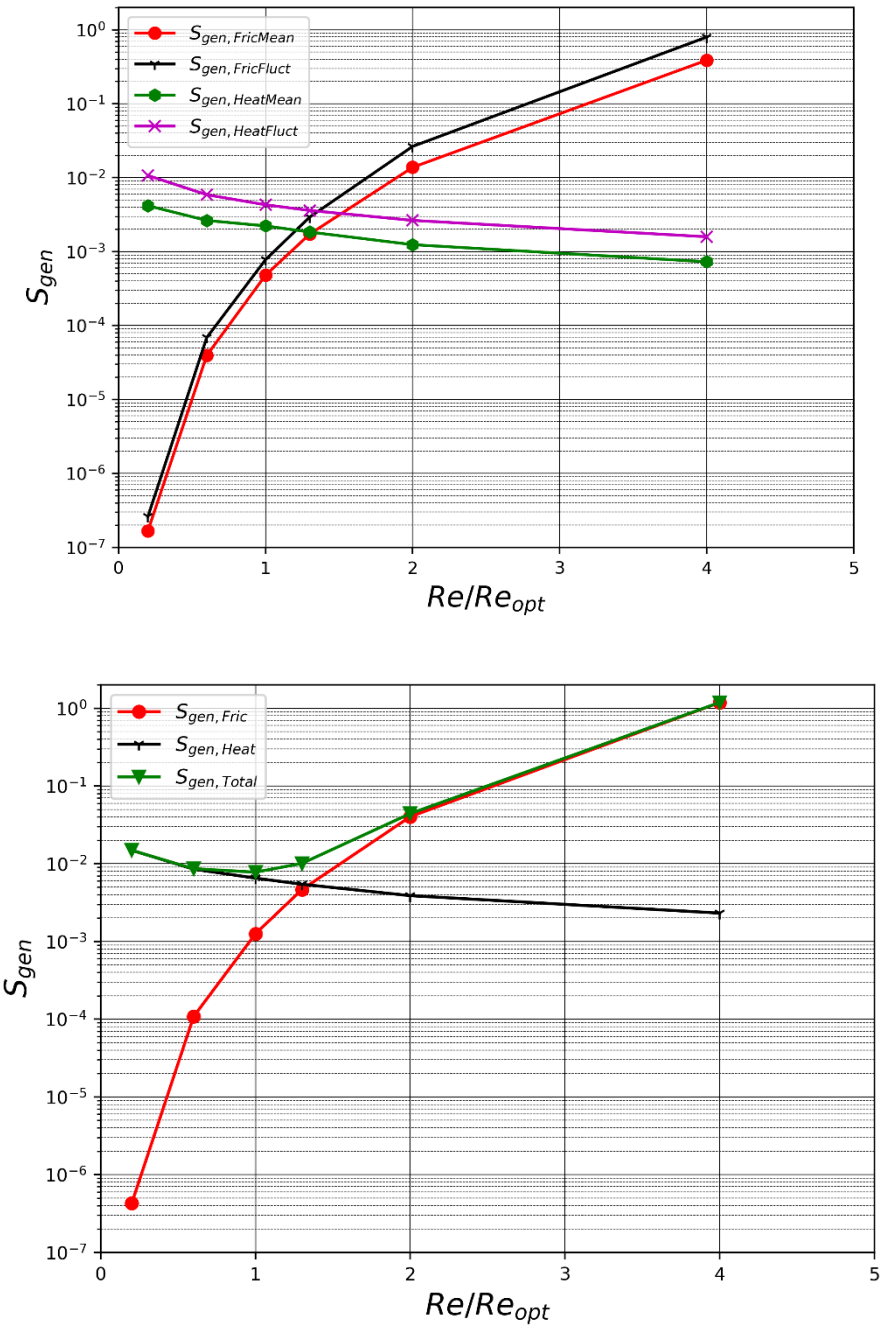

Figure 5.15. Entropy production terms

We can recognize that fluctuating components are greater than mean components of entropy production in all range of Re numbers, but they have the same behavior as their corresponding mean components. With increasing Re number friction component increases while heat component reduces intersecting at certain point. We can notice one more interesting point, the slope at which the entropy generation due to heat transfer changes are

much lower than the slope in case of entropy production due to friction, meaning that entropy generation due to temperature gradient is less sensitive to Re number changes than friction component of entropy generation.

CHAPTER 6
CONCLUSION

Concentrated Solar Panels technology is considered one of the promising solar power generation systems especially for the large scale power generation. The idea behind this technology is to concentrate large amounts of solar rays into a point (in case of solar power tower) or into a line (in case of parabolic trough) named collector or receiver. Thus, fluid flowing within the collector transfers the heat of solar rays to heat engine, which usually is a steam turbine. Nowadays solar salts or organic fluids are mainly used as a heat transfer fluids in CSP. In current thesis particular attention is given in to liquid metals by highlighting their advantages. According to the research conducted, liquid metals are proposed as an advanced high temperature transfer fluids because of superior thermal conductivity, high chemical stability at elevated temperatures (which cannot be said for organic fluids) and wide range of temperatures at which fluid remains in liquid phase.

From this research and analysis we can make few conclusions, the first one is to understand that the lower is the Prandtl number of the liquid the lesser entropy it will generate at its optimal Reynolds number. This information can be very useful since it will lead to operation of concentrated solar panels at higher efficiency, eventually it is one of the most important parameters in the design of the system. Second one, based on the results obtained, we can say that more uniformly the tube is heated the better effect it has on efficiency, especially if we operate our system at small Reynolds numbers where entropy generation due to heat transfer dominates.

One thing we should keep in mind, there is always a minimum point of entropy generation for given fluid type, and that point is represented by optimum Reynolds number. We should operate our system as close as possible to that point. For given diameter of receiver tube, fluid type and knowing operating conditions we can compute optimal velocity

of the fluid inside the receiver in a way described in current study and control it, thus we will keep our system at highest efficiency.

Concentrated solar panels possesses very big potential in energy sector, thus it is worth to investigate the possibilities of improving the performance of this technology, and that was the primarily objective of this thesis.

References

[1] S. Šarić, “Improved Modeling of Near-Wall Heat Transport for Cooling of Electric and Hybrid Powertrain Components by High Prandtl Number Flow”, 2017.

[2] C. Irrenfried, “Direct numerical simulation of turbulent heated pipe flow at high Prandtl numbers”, Graz University of Technology, 2013.

[3] H. K. Versteeg, W. Malalasekera, “An Introduction to Computational Fluid Dynamics, THE FINITE VOLUME METHOD, Second Edition”, PEARSON Prentice Hall, 2007.

[4] A. Bejan, “Entropy Generation Minimization: The Method of Thermodynamic Optimization of Finite-Size Systems and Finite-Time Processes (Mechanical and Aerospace Engineering Series)”, CRC Press, 1995.

[5] H. Herwig, F. Kock, “Direct and indirect methods of calculating entropy generation rates in turbulent convective heat transfer problems”, Springer-Verlag, 2006.

[6] A. Bejan, “Entropy generation minimization.” CRC Press, Boca Raton, 1996.

[7] R. J. A. Howard , “A wall heat transfer function for equilibrium flows – a combination of Reichardt and Kader profiles with Wang type scaling”, Begell House, 2012.

[8] J. Pacio, L. Marocco, Th. Wetzel, “Review of data and correlations for turbulent forced convective heat transfer of liquid metals in pipes”, Springer-Verlag Berlin Heidelberg, 2014.

[9] B. Gschaider, “Contrib/groovyBC”, https://openfoamwiki.net/index.php/Contrib /groovyBC, OpenFOAM wiki, 2015.

[10] B. Gschaider, “Contrib/funkySetFields”, https://openfoamwiki.net/index.php/ Contrib/funkySetFields, OpenFOAM wiki, 2015.

[11] C. J. Greenshield, “OpenFOAM, The Open Source CFD Toolbox Programmer’s Guide, Version 3.0.1”, CFD Direct Ltd, 2015.

[12] L. Marocco , G. Cammi , J. Flesch, Th. Wetzel, “Numerical analysis of a solar tower receiver tube operated with liquid metals”, International Journal of Thermal Sciences, 2016.

[13] J. Flesch, L. Marocco, A. Fritsch, K. Niedermeier, T. Wetzel, “Entropy generation minimization analysis of Solar Salt, sodium and lead-bismuth eutectic as high temperature heat transfer fluids”, Research Paper, 2018.

[14] F. Kock, H. Herwig, “Local entropy production in turbulent shear flows: a high-Reynolds number model with wall functions”, Hamburg, 2003.

[15] J. W. Slater, “Examining Spatial (Grid) Convergence”, https://www.grc.nasa.gov /www/wind/valid/tutorial/spatconv.html, NPARC Alliance Policy, 2008.

[16] ESI Group, “User Guide”, https://www.openfoam.com/documentation/user-guide/, OpenCFD Ltd, 2016-2018.

[17] Wikipedia, the free encyclopedia, “Dyadics”, https://en.wikipedia.org/wiki/ Dyadics, 2019.

[18] Wikipedia, the free encyclopedia, “Kármán Vortex Street”, https://en.wikipedia.org/ wiki/K%C3%A1rm%C3%A1n_vortex_street, 2019.

[19] CFD Online, “Turbulence intensity”, https://www.cfd-online.com/Wiki/Turbulence _intensity, GNU Free Documentation, 2018.